scientific reports

Check for updates

OPEN

A self-adjuvanted VLPs-based Covid-19 vaccine proven versatile, safe, and highly protective

Larissa Vuitika[1], Nelson Côrtes[1,2,10], Vanessa B. Malaquias[3,4], Jaqueline D. Q. Silva[1,3,4,10], Aline Lira[1,2,10], Wasim A. Prates-Syed[1,2,10], Lena F. Schimke[1,5], Daniela Luz[6], Ricardo Durães-Carvalho[7,12,13], Andrea Balan[8], Niels O. S. Câmara[1,14], Otavio Cabral-Marques[1,5,11], José E. Krieger[9], Mario H. Hirata[3,4] & Gustavo Cabral-Miranda[1,2,4,10]✉

Vaccination has played a critical role in mitigating COVID-19. Despite the availability of licensed vaccines, there remains a pressing need for improved vaccine platforms that provide high protection, safety, and versatility, while also reducing vaccine costs. In response to these challenges, our aim is to create a self-adjuvanted vaccine against SARS-CoV-2, utilizing Virus-Like Particles (VLPs) as the foundation. To achieve this, we produced bacteriophage (Qβ) VLPs in a prokaryotic system and purified them using a rapid and cost-effective strategy involving organic solvents. This method aims to solubilize lipids and components of the cell membrane to eliminate endotoxins present in bacterial samples. For vaccine formulation, Receptor Binding Domain (RBD) antigens were conjugated using chemical crosslinkers, a process compatible with Good Manufacturing Practice (GMP) standards. Transmission Electron Microscopy (TEM) confirmed the expected folding and spatial configuration of the QβVLPs vaccine. Additionally, vaccine formulation assessment involved SDS-PAGE stained with Coomassie Brilliant Blue, Western blotting, and stereomicroscopic experiments. In vitro and in vivo evaluations of the vaccine formulation were conducted to assess its capacity to induce a protective immune response without causing side effects. Vaccine doses of 20 µg and 50 µg stimulated the production of neutralizing antibodies. In in vivo testing, the group of animals vaccinated with 50 µg of vaccine formulation provided complete protection against virus infection, maintaining stable body weight without showing signs of disease. In conclusion, the QβVLPs-RBD vaccine has proven to be effective and safe, eliminating the necessity for supplementary adjuvants and offering a financially feasible approach. Moreover, this vaccine platform demonstrates flexibility in targeting Variants of Concern (VOCs) via established conjugation protocols with VLPs.

Keywords VLPs platform, Vaccine, SARS-CoV-2, COVID-19

[1]Department of Immunology, Institute of Biomedical Sciences, University of São Paulo, São Paulo, Brazil. [2]The Interunits Graduate Program in Biotechnology, University of São Paulo, the Butantan Institute and the Technological Research Institute of the State of São Paulo, São Paulo, Brazil. [3]Department of Clinical and Toxicological Analyses, School of Pharmaceutical Sciences, University of Sao Paulo, São Paulo, Brazil. [4]The Graduate Program in Pathophysiology and Toxicology, Department of Clinical and Toxicological Analyses, School of Pharmaceutical Sciences, University of São Paulo, São Paulo, Brazil. [5]Department of Medicine, Division of Molecular Medicine, Laboratory of Medical Investigation 29., University of São Paulo School of Medicine, São Paulo, Brazil. [6]Laboratory of Bacteriology, Butantan Institute, São Paulo, Brazil. [7]São Paulo School of Medicine, Department of Microbiology, Immunology and Parasitology, Federal University of São Paulo (UNIFESP), São Paulo, SP, Brazil. [8]Applied Structural Biology Laboratory, Institute of Biomedical Sciences, University of São Paulo, São Paulo 05508-000, Brazil. [9]Heart Institute, Clinical Hospital, Faculty of Medicine, Laboratory of Genetics and Molecular Cardiology, Clinical Hospital, Faculty of Medicine, University of São Paulo, São Paulo, Brazil. [10]Department of Infectious Diseases and Tropical Medicine, Faculty of Medicine, University of São Paulo, São Paulo, Brazil. [11]DO'R Institute for research, São Paulo, Brazil, IDOR, São Paulo, Brazil. [12]Department of Morphology and Genetics, Federal University of São Paulo, São Paulo, Brazil. [13]Interunit Bioinformatics Graduate Program, Institute of Chemistry, University of São Paulo, São Paulo, Brazil. [14]Nephrology Division, Department of Medicine, Federal University of São Paulo, São Paulo, Brazil. ✉email: gcabral.miranda@usp.br; gcabral.miranda@gmail.com

SARS-CoV-2 (Severe Acute Respiratory Syndrome Coronavirus 2), the causative agent of COVID-19 (Coronavirus Disease 2019)[1], was responsible for a global pandemic resulting in over 775 million cases and 7 million deaths[2]. While no longer considered a public health emergency of international concern, the World Health Organization (WHO) has emphasized that the persistent nature of the pandemic highlights the crucial need for long-term management strategies for SARS-CoV-2. Continuous vaccination campaigns are imperative until either the emergence of new variants of concern (VOCs) ceases or vaccines provide lasting immunity[3–5].

Coronaviruses like SARS-CoV-2 enter host cells by attaching to Spike glycoproteins (S proteins) on their surface[6]. The Receptor Binding Domain (RBD) of the Spike protein binds to host cell receptors, making it the primary target for anti-SARS-CoV-2 vaccine development. Patients who recover from infection often have neutralizing antibodies targeting the Spike protein, particularly the RBD, in their blood[7,8]. Among vaccine platforms, subunit antigens are widely acknowledged as one of the safest and most effective strategies for vaccine development[9]. However, they do not inherently generate a strong immune response and require the use of adjuvants in vaccine formulations[10], most of which only moderately inducing the Th1 immune response crucial for combating viral infections like COVID-19[11]. Additionally, the availability of adjuvants is limited - only a small number is licensed for human use – and their use increases vaccine costs.

Virus-like particles (VLPs) are emerging as an exceptionally promising vaccine platform due to their ability to generate potent and long-lasting immune responses[12–14]. Unlike traditional vaccines and newer technologies such as viral vector and mRNA vaccines, VLPs do not contain viral genetic material, thus eliminating the risks associated with replication and transmission, and enhancing safety. Their structural similarity to actual viruses enables VLPs to effectively engage both B and T cells through antigen-presenting cells (APCs), resulting in a robust and sustained immune reaction. VLPs also offer significant advantages in terms of stability, versatility, and ease of production, potentially reducing both costs and manufacturing time compared to other platforms. Additionally, VLPs' ability to mimic viral surface proteins and present them as pathogen-associated molecular patterns (PAMPs) allows for a highly effective immune response and memory development. Their stability, lack of allergenicity, and adaptability to various expression systems—such as bacteria, yeast, and mammalian cells—make them suitable for a wide range of applications, including vaccines for SARS-CoV-2, HIV, Ebola, Dengue, Chikungunya, etc. These attributes make VLPs a significant choice among both traditional and emerging vaccine technologies, combining high safety and immunogenicity with practical production advantages[15–19].

Several vaccines based on VLPs have already been licensed and are commercially available for diseases such as Hepatitis B (Engerix-B® and Recombivax HB®), Human Papillomavirus (Gardasil® and Cervarix®), Hepatitis E (Hecolin®), and Malaria (Mosquirix™)[20]. At present, multiple vaccine candidates based on VLPs are being tested in clinical and preclinical trials across different expression systems, targeting a range of infectious diseases and other health conditions[16,21–25].

Given the persistent global efforts to address COVID-19, there is a pressing need to investigate novel vaccine strategies to overcome current challenges. Recent developments in vaccine technology have demonstrated the potential of VLPs as an effective and safe vaccine platform. VLPs-based vaccines have already shown success in combating other infectious diseases, evidencing their capability to elicit strong immune responses and provide sustained protection. This context highlights the importance of further research into VLP-based vaccines for COVID-19, focusing on improving their efficacy and minimizing the need for additional adjuvants. This study contributes to this effort by developing a self-adjuvanted VLP-based vaccine for COVID-19, utilizing the inherent strengths of VLPs to stimulate a robust immune response against SARS-CoV-2 while addressing the limitations of existing vaccine approaches.

Materials and methods

Experimental design

The Covid-19 vaccine investigated in this study was developed through a systematic three-step experimental approach, as outlined in the flowchart (Fig. 1) of the experimental design. Step 1 entailed an understanding of the antigen utilized, specifically the RBD of the Spike protein. We then evaluated the use of VLPs that could be produced efficiently under favorable conditions, characterized by low cost and high immunogenicity. Additionally, the antigen needed to be readily conjugated to the VLPs using a simple and replicable strategy. For this purpose, we selected Qbeta bacteriophage (Qβ) VLPs due to their exposed lysine amino groups, which are well-suited for antigen coupling via bifunctional crosslinkers without disrupting VLPs self-assembly. The vaccine was subsequently formulated and characterized, as detailed in the section "Production and Characterization of the VLPs-Based Vaccine."

In Step 2, we aimed to determine the optimal vaccine dose and assess the immunological response induced. For this, isogenic C57BL/6 mice were employed to evaluate both the humoral and cellular immune responses elicited by the vaccine formulation, along with the ability of the antibodies to neutralize SARS-CoV-2. The final phase, Step 3, also involved C57BL/6 mice, but specifically those genetically modified to express human ACE2 (human ACE2 knock-in mice). The reasons behind the choice of such an approach are two-fold: to provide consistency of experimental lineage, allowing comparative analysis with previous results, and to adopt a model that expressed the relevant receptor for SARS-CoV-2 infection, facilitating a more accurate assessment of the vaccine's protective efficacy. Mice were vaccinated with the most effective doses identified from prior experiments. Following vaccination, the mice were challenged with SARS-CoV-2 as described. Clinical signs were monitored, and at the conclusion of the study, viral load and potential tissue damage in the lungs of both vaccinated and unvaccinated challenged mice were evaluated and compared to a control group that was not challenged.

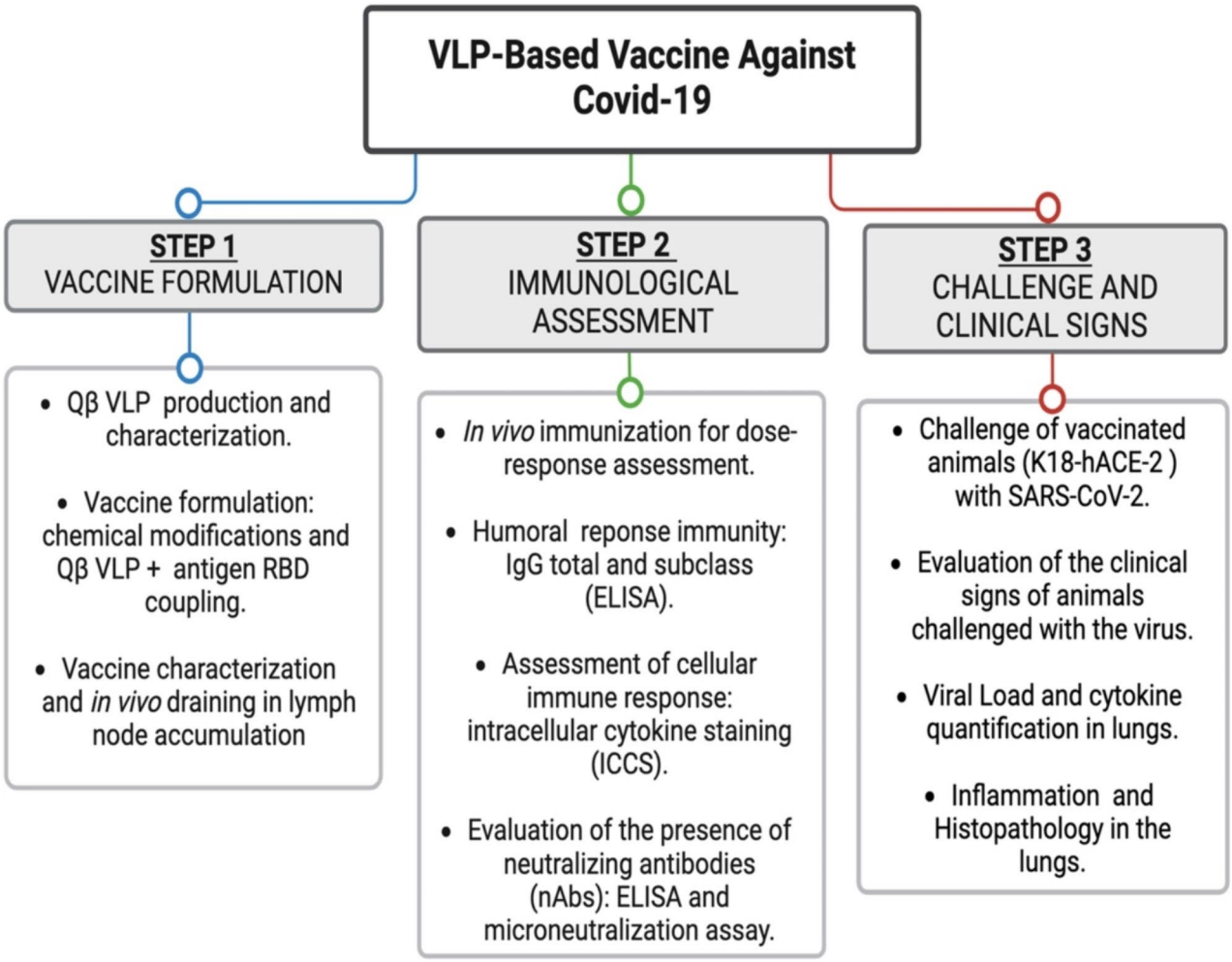

Fig. 1. Flowchart of the experimental design.

Production and characterization of the VLPs-based vaccine

The vaccine was produced using the QβVLPs, based on the coat protein (CP) which forms a uniform VLPs, with an encapsulated toll-like agonist (Fig. 2A and B). For that, synthetic *E. coli* plasmid of the QβVLPs was constructed by Creative Biostructure (Ramsey Road Shirley, NY 11967, USA), cloning the CP gene from Qβ bacteriophage into pET28a(+) without a 6x-His tag. The constructed plasmid was then used to transform BL21 (DE3) *E.coli* competent cells obtained from Thermo Fisher Scientific. Recombinant expression of the QβVLPs was carried out in Hannahan's Broth (SOB medium) for 16 h at 30 °C and 200 rpm. When the optical density at 600 nm (OD600nm) reached 0.6, 1 mM IPTG was added to induce protein expression. After induction, the bacterial cell suspension was centrifuged at 5,000 rpm for 15 min, and the resulting cellular sediment was resuspended in PBS. Subsequently, the cells were lysed by sonication for 15 min using a 35% potency (10 s on and 15 s off). The lysate was then centrifuged, and both the supernatant and pellet fractions were analyzed using SDS-PAGE to assess protein expression. For purification of the QβVLPs, 10% (w/v) PEG 8,000 was added to the supernatant fraction, and the mixture was incubated overnight on a nutating mixer at 4 °C to precipitate total proteins. The precipitate was collected by centrifugation at 9,000 rpm for 30 min. The resulting pellet was resuspended in PBS at pH 7.2 and mixed with an equal volume of a 1:1 chloroform/isobutanol mixture until it formed a colloid. The mixture was then centrifuged at 9,000 rpm for 1 h to separate the layers. The top (aqueous) layer was collected, and dialysis with PBS at pH 7.2 was performed to remove any remaining organic solution.

The total QβVLPs were quantified using the Pierce BCA Protein Assay kit from Thermo Scientific, USA. The purity of the QβVLPs was assessed using SDS-PAGE, Western blotting, and transmission electron microscopy (TEM) (Fig. 2 C-E).

To conjugate the RBD protein to Qβ VLPs, chemical modifications were performed based on established protocols with modifications[26–29]. Initially, the RBD protein was incubated with a 7.5-fold excess of SATA (N-succinimidyl-S-acetylthioacetate) for 30 min. Excess SATA was removed by diafiltration, and hydroxylamine hydrochloride was subsequently added at a 1:10 (v/v) ratio. The mixture was incubated at room temperature for three hours to introduce reactive sulfhydryl groups into the RBD protein. Following this, the excess

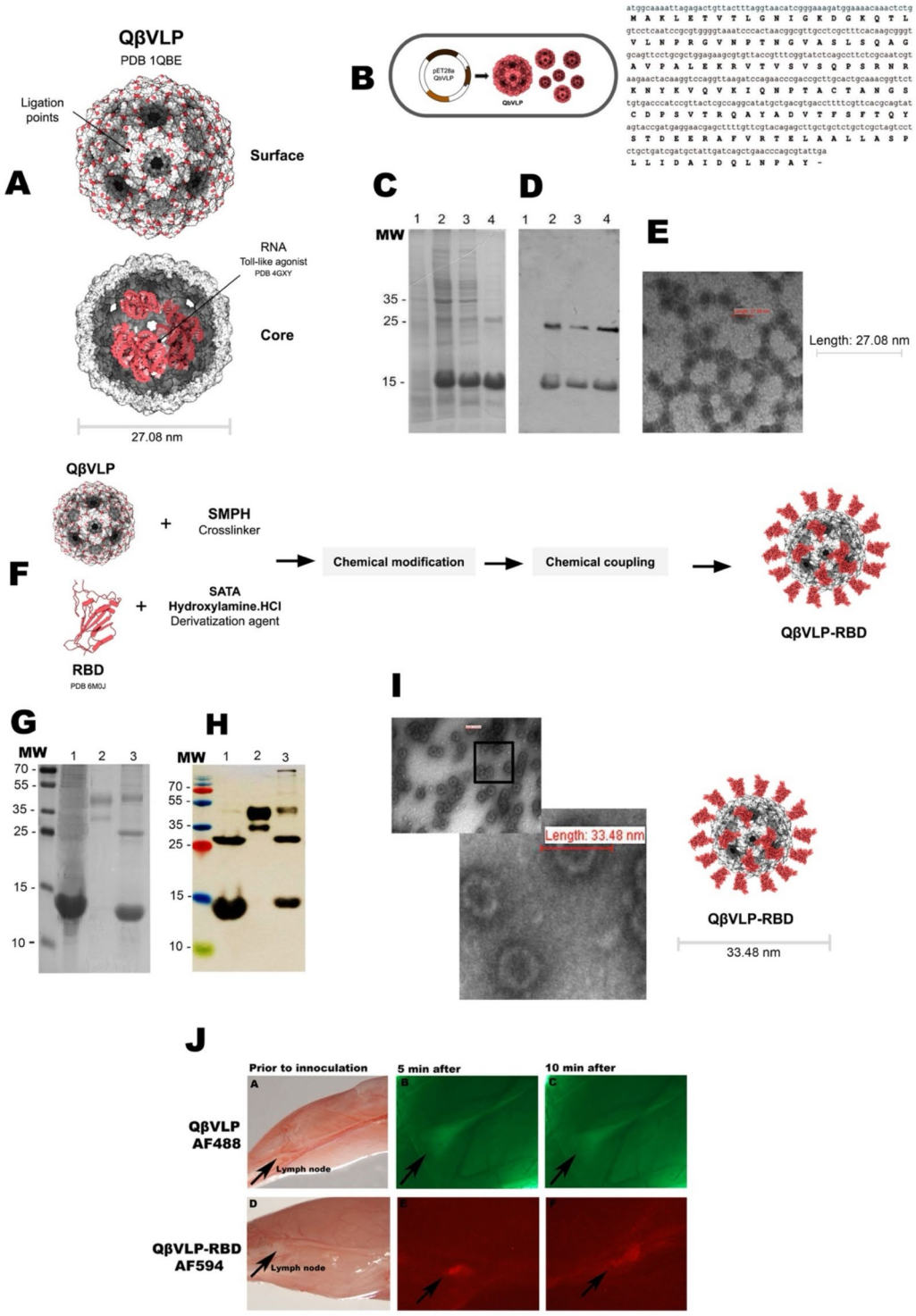

hydroxylamine hydrochloride was removed, and the protein was dialyzed against PES buffer (20 mM sodium phosphate, 2 mM EDTA, and 30% (w/v) sucrose, pH 7.2).

The purified QβVLPs were then treated with SMPH (succinimidyl-6-(b-maleimidopropionamido) hexanoate) cross-linker at a 10-fold molar excess and incubated at room temperature for 30 min. Unreacted SMPH was removed by diafiltration, and the VLPs were dialyzed with PES buffer. Subsequently, the RBD protein, prepared with sulfhydryl groups, was mixed with the SMPH-activated QβVLPs in equimolar amounts. The conjugation reaction was allowed to proceed for four hours at room temperature to achieve covalent linkage of the RBD protein to the QβVLPs.

The vaccine formulation was analyzed using 15% SDS-PAGE under reducing conditions, followed by Coomassie brilliant blue staining. For western blot analysis, the gels were electro blotted onto nitrocellulose membranes (Bio Rad, USA) using Trans-Blot® SD Semi-Dry Transfer Cell Blots (Bio Rad, USA). Besides, aliquots

◀**Fig. 2**. VLPs-based vaccine production and characterization. (**A**) The QβVLPs (PDB 1QBE) tridimensional structures, highlighting the high exposure number of linker conjugation points, as well as the internal toll-like agonist and the core with ~27 nm, measured after electron microscopy analysis (**E**). (**B**) The coat protein gene of Qβ bacteriophage (Genbank M99039.1 and Proteinbank AAA1662.1) was cloned in pET28a and BL21 (DE3) *E. coli* competent cells were transformed with the construction. After IPTG induction QβVLPs are self-assembled in the bacteria cytoplasm. (**C**) The expression and purification of recombinant QβVLPs was analyzed using 15% SDS–PAGE under reducing conditions and Coomassie blue dye staining. Line 1 depicts E. coli cells before induction with 1 mM IPTG. Lane 2 shows the proteins of cells after induction IPTG. Lanes 3 depict the supernatant (soluble form) obtained through freeze, thawing and sonication lysis in the extraction buffer before purification. Lane 4 show purified recombinant protein CP Qβs. (**D**) Western blot of the bacterial extracts and purified CP QβVLPs using hyperimmune serum of the mouse immunized with QβVLPs. Line 1 depicts E. coli cells before induction with 1 mM IPTG. Lane 2 shows the proteins of cells after induction IPTG. Lanes 3 depict the supernatant (soluble form) after lysis. Lane 4 show purified recombinant protein CP QβVLPs. Molecular weight marker (Thermo Fisher Scientific Ref. 26619). (**E**) Transmission electron microscopy (EM) of QβVLPs nanoparticle at 129.300 magnitude. (**F**) Chemical modifications performed on the QβVLPs (SMPH) and RBD antigen (SATA and Hydroxylamine.HCl), and subsequent conjugation for the vaccine formulation. Bacteriophage Q beta capsid protein in T3 symmetry PDB Entry − 7TJM; SARS-CoV-2 E406W mutant RBD PDB Entry − 7TPK (**G**) SDS-PAGE 15% stained with Coomassie brilliant blue for characterization of the vaccine formulation. Line 1 QβVLPs, line 2 RBD antigen and line 3 the vaccine profile with different bands representing different vaccine oligomers. (**H**) Western blot performed with hyperimmune serum anti QβVLP-RBD vaccine and total anti-mouse IgG antibody conjugated with HRP. Line 1 QβVLPs, line 2 RBD antigen, line 3 shows the vaccine profile with different bands representing different vaccine oligomers. (**I**) Transmission EM of the VLPs-based vaccine and its tridimensional structure. (**J**) Stereomicroscopic images of popliteal draining LN in live mice illustrate the accumulation of QβVLPs labeled with AF488 QβVLPs-RBD vaccine labeled with AF594 (A-bright field image of LN (identified by arrowhead); **B**-**C** QβVLPs/AF488 in 5 and 10 min post injection taken with appropriate fluorescent filter sets; **D**-**E** QβVLPs-RBD vaccine/AF594 in 5 and 10 min and post injection taken with appropriate fluorescent filter sets. Magnitude 7x. The QβVLPs (PDB 1QBE) (https://doi.org/10.1016/s0969-2126(96)00060-3), RBD (PDB 6M0J) (https://doi.org/10.1038/s41586-020-2180-5), and the RNA (PDB 4GXY) (https://doi.org/10.1038/nsmb.2405) tridimensional structures were rendered on 3D protein imager (https://doi.org/10.1093/bioinformatics/btaa009).

of QβVLPs alone or QβVLPs displaying RBD were used to be analyzed by TEM. For that, the samples were diluted to a concentration of 0.5 µg/µL, and subsequently applied to glow-discharged, carbon-coated Formvar copper grids obtained from Electron Microscopy Sciences[30]. The dried grids were then examined usin a LEO 906E transmission electron microscope from Zeiss, Germany, operating at an acceleration voltage of 80 kV. Images were acquired at a magnification of 129, 300x.

Stereomicroscopic imaging was performed to analyze the trafficking of the VLPs alone and the vaccine formulation to lymph nodes of mice, as previously described[15,30]. For that, QβVLPs alone and QβVLPs-RBD were labeled with hyperimmune anti- QβVLPs and anti-RBD and subsequently labeled with Alexa Fluor 488 (AF488) and Alexa Fluor 594 (AF594), according to the manufacturer's instructions (Thermo Fisher Scientific). The particles were injected subcutaneously (s.c.) into the C57BL/6 mice footpad and measured the draining kinetics. Fluorescent light illumination with a ZEISS Axio Zoom.V16 camera was used for imaging.

Procedures involving animals

All animal experiments in this study were performed in accordance with relevant guidelines and regulations, adhering to Brazilian Federal Law 11.794, which regulates the scientific use of animals, and State Law 11.977, the Animal Protection Code of São Paulo. The project protocol received approval from the Animal Ethics Committee (CEUA) of the Institute of Biomedical Sciences, University of São Paulo (Protocol number 133290720). This study is reported in accordance with ARRIVE guidelines to ensure comprehensive oversight, maximizing research quality, reliability, and transparency.

C57BL/6 mice were purchased from the Central Animal Facility of the Faculty of Medicine at the University of São Paulo, while knockin human ACE2 (B6.Cg-Tg(K18-ACE2)2Prlmn/) mice were obtained from "The Jackson Laboratory," Bar Harbor, Maine, USA. Animals were housed in ventilated autoclaved cages (Alesco, Brazil) under specific pathogen-free conditions with controlled temperature, humidity, and a 12:12 light-dark cycle. In scientific studies involving the mice, the use of ketamine (100 mg/kg) and xylazine (10 mg/kg) were implemented for anesthesia, offering effective sedation and analgesia. This combination enhances safe handling and reduces stress during experimental procedures. Furthermore, isoflurane served as an inhalational anesthetic for both short and prolonged procedures, ensuring consistent maintenance of anesthesia and stable physiological conditions throughout the study.

At the conclusion of each experiment, animals were humanely euthanized using an approved Schedule 1 method (cervical dislocation). These practices uphold ethical standards and ensure compliance with animal welfare regulations throughout the study.

Assessment of the immunological capacity generated by the vaccine formulation

To assess the capacity of the VLPs-based vaccine to induce humoral and cellular immune response, as well as neutralizing antibodies against the SARS-CoV-2, experiments were conducted using female C57BL/6 mice, and

knockin human ACE2 (B6.Cg-Tg(K18-ACE2)2Prlmn/) strains, aged between 6 and 8 weeks (mature immune system).

The vaccination was applied subcutaneously (s.c.) with varying doses of the QβVLPs-RBD vaccine. Initially, we administered sequential doses of the vaccine formulation at 2.5 µg, 5 µg, 10 µg, and 20 µg to assess their efficacy in eliciting an immune response. The doses of 2.5 µg, 5 µg, and 10 µg did not generate a sufficiently robust immunological response. Therefore, we proceeded with the higher doses and included an additional group receiving 50 µg. The 50 µg dose demonstrated a significantly enhanced ability to induce immunity in the murine model. Based on these results, the 20 and 50 µg doses were selected for further investigation due to its superior immunogenicity. As controls, separate groups of mice were immunized with only QβVLPs, RBD, or PBS. The immunizations were administered in two doses, with 14 days of interval between each injection.

To measure the antibody response, blood samples were collected via cheek vein puncture on days 0 (prior vaccination), 7, 14 after the first immunization, and days 7 and 14 after the boost. Following sample collection, all mice were humanely euthanized through CO_2 exposure. We performed three independent experiments, with each arm consisting of five female mice, resulting in a total of 15 mice per group.

The production of IgG antibodies, including total and subclass-specific responses, was evaluated using enzyme-linked immunosorbent assays (ELISA), following established protocols with minor modifications[26–30]. Recombinant Spike protein was diluted to 1 µg/mL in 50 mM carbonate buffer (pH 9.6) and used to coat ELISA plates, which were incubated overnight at 4 °C. The next day, the plates were washed three times with PBS containing 0.05% Tween 20 and subsequently blocked with 1% PBS-BSA for two hours. After blocking, mouse serum samples were added to the plates, starting with a 1:150 dilution, followed by serial three-fold dilutions (1:3) up to four times. The plates were then incubated with goat anti-mouse total IgG HRP conjugate (Sigma-Aldrich/Merck, USA) as the secondary antibody. For subtype identification, goat anti-mouse IgG1 and IgG2b antibodies (Sigma-Aldrich/Merck, USA) were employed. The reaction was developed by adding 100 µL of TMB substrate (Sigma-Aldrich/Merck, USA) to each well and incubating for 10 min at room temperature in the dark. The reaction was halted with 0.5 M H2SO4, and optical density was measured at 450 nm using a microplate reader.

The neutralizing capacity of antibodies was assessed by evaluating the ability of hyperimmune serum from vaccinated mice to inhibit the binding of the RBD to human hACE2. This was performed using the cPass SARS-CoV-2 Neutralization Antibody Detection Kit (GenScript, USA). Serum samples were collected 14 days after the second dose of the QβVLPs-RBD vaccine (administered at 20 µg and 50 µg) and tested alongside controls including QβVLPs, RBD, and PBS. The kit's provided negative and positive controls were prepared as per the manufacturer's instructions. For the assay, serum samples were diluted 1:10 and mixed with HRP-conjugated RBD. This mixture was incubated at room temperature for 1 h, then added to a 96-well microplate coated with hACE2. After a 15-minute incubation at room temperature, the microplate was washed with the specific buffer provided by the kit. The reaction was developed by adding the TMB substrate from the kit and was stopped with the provided acidic solution. The absorbance was then measured at 450 nm using a microplate reader.

In addition to utilizing the commercial kit, we conducted an in vitro neutralization assay with SARS-CoV-2 to further evaluate the neutralizing efficacy of serum from vaccinated and control mice. This assay adhered to a well-established and published protocol[31], with specific modifications, to ensure the accuracy and reliability of antibody neutralization against the native virus. Serum samples were first heat-inactivated at 56 °C for 1 h to eliminate complement activity. Vero E6 cells, cultured in DMEM supplemented with 5% FBS, were seeded at 10^4 cells per well in 96-well plates and incubated for 24 h at 37 °C in 5% CO2 to allow for cell adhesion. Serum samples, collected 14 days after the booster dose, were initially diluted 1:20, followed by serial three-fold dilutions (1:3) up to four times. These diluted sera were then incubated with 100 TCID50 of SARS-CoV-2 P.1 (Gamma variant, GenBank: MW642250.1) for 1 h at 37 °C. Following incubation, the virus-serum mixtures were added to the Vero E6 cell plates in DMEM with 1% FBS and further incubated for 72 h at 37 °C in 5% CO2. Negative controls (cells without serum and virus) and positive controls (cells with virus only) were included. After 72 h, the plates were washed and fixed with 4% paraformaldehyde for 20 min. Paraformaldehyde was removed, and the cells were stained with 0.5% crystal violet for 30 min. The excess dye was then washed away with PBS, and the plates were dried before being immersed in methanol. Absorbance was measured at 620 nm using a microplate reader. The experiments were performed in triplicate across three independent assays to ensure reproducibility and reliability of the results.

Cellular immune response was evaluated by intracellular cytokine staining (ICCS). The spleen and lymph nodes of mice were collected two weeks after the boost immunization with VLPs-based vaccine, QβVLPs alone, RBD protein, or PBS. The organs were macerated using a Potter homogenizer. The extracted cells were filtered through a 40 µm cell strainer (Corning, EUA), washed with PBS, and then plated in a 96-well microplate at a concentration of 1×10^6 cells/mL in RPMI-1640 medium supplemented with 10% FBS. For the positive control, cells were incubated with a stimulus solution of PMA + ionomycin in the presence of brefeldin A Stop Golgi (BD Bioscience, USA). The negative control cells were treated with PBS + brefeldin A Stop Golgi. To detect cytokines, T cells from the immunized mice were incubated with 5 µg of RBD + brefeldin A Stop Golgi®. All samples were then incubated for 12 h at 37 °C in a 5% CO_2 environment. After incubation, th cells were fixed and permeabilized using the Cytofix/Cytoperm™ Plus Fixation/Permeabilization kit (BD Biosciences, USA). They were then stained with anti-mouse $CD4^+$ (BD Bioscience, USA), anti-mouse $CD8^+$ (BD Bioscience, USA), and anti-mouse IFNγ (BD Bioscience, USA) antibodies. Cytometry analysis was performed using the FACS Canto II flow cytometer (BD Biosciences, EUA), and the data were analyzed using FlwJo software (Flowjo, EUA, https://www.flowjo.com/solutions/flowjo) and GraphPad Prism 9.1 (Graphpad Software, EUA https://www.graphpad.com/).

Measuring vaccine protective capacity and safety

Following evaluation of immune induction capacity of the vaccine formulation, we measured protection against viral infection and safety. Female B6.Cg-Tg(K18-ACE2)2Prlmn mice were vaccinated and challenged with P1. SARS-CoV-2. Prior to vaccination, the B6.Cg-Tg(K18-ACE2)2Prlmn mice were genotyped according to The Jackson Laboratory recommendations. Each group consisting of five animals were vaccinated as described previously. On the 35th day following the immunization schedule, the animals were intranasally challenged with 10^6 virus particles of P.1 SARS-CoV-2 diluted in 40 µL of PBS. Clinical signs, behavior, and weight loss were monitored for seven days.

Following the observation period, the right lung of each animal was collected and preserved in 10% formalin solution buffered with phosphate for a duration of seven days. The lung specimens were then embedded in paraffin and processed using a tissue processor (PT05 TS, LUPETEC, UK). Subsequently, histological paraffin (Histosec, Sigma-Aldrich) was used to embed the lung samples. Thin sections measuring 4 µm in thickness were prepared and stained with hematoxylin and eosin. The resulting sections were captured using a Slide Digitizer – 3D Histech scanner and subsequently analyzed using Download CaseViewer 2.4, 64-bit version (3D-Histotech, Hungary) - https://www.3dhistech.com/solutions/caseviewer/). Finally, the figures were compiled using Adobe Photoshop version 23.5.4 (USA, https://www.adobe.com/br/products/photoshop.html).

Viral quantification was measured by qRT-PCR. Total RNA was extracted from homogenized mice lungs using Trizol Reagent. To synthesize cDNA, the Superscript II Reverse Transcriptase (Thermo Fisher) was employed, in accordance with the manufacturer's instructions. Real-time PCR was conducted using the Power SyBr green master mix (Thermo Fisher) and a QuantStudio 12k thermocycler (Thermo Fisher), utilizing the following parameters: an initial denaturation step at 95 °C for 15 min, followed by 40 cycles of denaturation at 95 °C for 15 s and annealing/extension at 60 °C for 1 min. The primer sequences used were as follows: CoV-2 forward 5′- GCCTCTTCTCGTTCCTCATCAC-3′ and CoV-2 reverse 5'- AGCAGCATCACCGCCATTG – 3'. The qRT-PCR data were presented as 1/ΔCT and were performed in triplicate.

In addition, we also measured the cytokine expression profile in the lung tissue of vaccinated and control animals by RT-qPCR. The assay was performed as described above for viral load quantification. The oligonucleotides used are shown in Table 1.

Statistical analysis

The statistical analysis of all data was conducted using GraphPad Prism 9.1 for Mac (GraphPad Inc, USA, https://www.graphpad.com/). For comparisons between two normally distributed groups, an unpaired t-test was utilized, taking into account the distribution of the data. Alternatively, when comparing two non-parametric groups, a Mann–Whitney rank test was applied. In cases involving more than two groups, non-parametric data were assessed using one-way ANOVA, with Bonferroni's multiple comparison post-test applied to normally distributed data. Weight measurements and flow cytometry data were subjected to analysis via Two-Way ANOVA. Survival analysis was performed using the log-rank test. Statistical significance was determined at $P \leq 0.05$.

Results

The production of VLPs-based vaccine platform

The strategy of this study involved generating QβVLPs in prokaryotic system (*E. coli*) to enable high-level production, rapid purification and evaluation of its solubility, stability, and ultrastructural morphology. The purification protocol included viral particle precipitation, clarifications with organic solvents, centrifugations, and dialysis[32,33], aiming to remove lipopolysaccharides (LPS) present in the bacterial samples used for the study. To validate this approach and assess the regulatory implications of including host-derived RNA in vaccine formulations, we conducted an endotoxin evaluation of the QβVLP vaccine using the Thermo Scientific™ Pierce™ Chromogenic Endotoxin Quant Kit, following the manufacturer's guidelines. The endotoxin concentration in the QβVLP vaccine was measured at 1.6 EU/mL. For reference, preclinical studies generally set the acceptable endotoxin threshold for recombinant vaccines at less than 20 EU/mL[34]. This simple, fast, and cost-effective purification method shows great promise for purifying QβVLPs nanoparticles.

The analysis of the production of recombinant QβVLPs is illustrated in Fig. 2. Figure 2 C displays two bands at approximately 15 kDa (monomer) and 30 kDa (dimer) after IPTG culture induction (Line 2), in the soluble form (Line 3), and after purification (Line 4). Western blot analysis using hyperimmune serum from mice immunized with QβVLPs confirms immune recognition of the 15 kDa (monomer) and 30 kDa (dimer) bands,

Gene	Oligonucleotides Sequences 5'-3'	
	Forward	Reverse
IL-1β	ACCTGTCCTGTGTAATGAAAGACG	TGGGTATTGCTTGGGATCCA
IFN-α	GTTCAAGTCTCTGTCCCCAAAA	GTGGGAACTGCACCTGATGT
IFN-β	CAGCTCCAAGAAAGGACGAAC	GGCAGTGTAACTCTTCTGCAT
TNF-α	CCCTCACACTCAGATCATCTTCT	GCTACGACGTGGGCTACAG
IL-6	TGTTCTCTGGGAAATCGTGGA	AAGTGCATCATCGTTGTTCATACA
IL-4	TCATCGGCATTTTGAACGAG	CGTTTGGCACATCCATCTCC

Table 1. Oligonucleotides sequences used to quantify cytokine mRNAs by RT-qPCR.

as expected (Fig. 2 D), corroborating the SDS-PAGE results. Notably, our QβVLPs were produced in the soluble form with a yield of 50 mg/L of purified recombinant protein.

Furthermore, our experimental data regarding the production of VLPs underwent analysis using TEM. The results of this analysis confirmed that the QβVLPs were correctly folded and displayed the appropriate spatial configuration (Fig. 2 E). Information regarding particle size distribution is crucial for comprehending product homogeneity. Figure 2E and I illustrate the uniform and non-aggregated morphology of both the VLPs nanoparticles alone and the QBVLPs vaccine conjugated with the RBD protein. These observations are consistent with findings from other studies that also report size homogeneity of VLPs nanoparticles as observed via TEM[30].

As part of the vaccine formulation utilizing the QβVLPs platform, we initially employed the commercial RBD (GenScript Ref. Z03483-1) as the viral antigen. Covalent conjugation of the RBD with QβVLPs was performed using equimolar amounts (Fig. 2 F). To evaluate the vaccine formulation, we employed 15% SDS-PAGE stained with Coomassie brilliant blue (Fig. 2 G), Western blotting (Fig. 2H), and TEM imaging (Fig. 2 I), as mentioned earlier. Additionally, the RBD conjugated to the VLPs underwent labeling with specific antibodies to perform stereomicroscopic experiments (Fig. 2 J). Analysis of Fig. 2 G and H, specifically line 3, reveals the composition of the vaccine formulation. The expected bands for QβVLPs at 15 kDa and the RBD protein at ~50 kDa are observed, along with additional bands of varying heights representing different couplings of molecules, such as dimers and trimers. The presence of a 50 kDa band corresponding to the RBD protein was observed in Western blot (Fig. 2H), recognized by the antibody from hyperimmune sera against QβVLPs-RBD vaccine. The presence of the RBD antigen in the vaccine formulation demonstrates that there was no degradation post-formulation, as further validated by TEM imaging (Fig. 2 I). As a result, the vaccine formulation was prepared to be evaluated in an animal model.

We further investigated the QβVLPs vaccine immunogenic potential by evaluating lymph node drainage dynamics through stereomicroscopic experiments, which provided insights into the kinetics of antigen drainage. The results showed rapid drainage and accumulation in the popliteal draining lymph node as early as 5 to 10 min post-injection (Fig. 2 J).

Immunological assessment of the VLPs-based vaccine formulation

Following the characterization of the vaccine candidate, we evaluated the humoral and cellular immune responses in animals that received two doses of the QβVLPs-RBD vaccine formulation at doses of 20 µg and 50 µg. The levels of total IgG and specific subclasses, IgG1 and IgG2b, binding to the recombinant Spike and RBD proteins of SARS-CoV-2 were measured by ELISA (Fig. 3 A).

The production of total IgG against the recombinant Spike protein was found to be dependent on both time and dosage (Fig. 3 B-C). We observed a significant increase in antibody production titers 14 days after the initial immunization, which further intensified after the booster dose (14 days after second immunization). Notably, the formulations of the QβVLPs-RBD vaccine with doses of 20 µg and 50 µg exhibited particularly significant increases in total IgG production. Additionally, a similar profile of total IgG presence was observed in hyperimmune serum samples from animals after 14 days of the vaccine boost, recognizing the RBD subunit (Fig. 3D).

Furthermore, we analyzed the IgG subclasses specific to the Spike recombinant protein, specifically IgG2b and IgG1. Figure 3E depicts an elevated level of IgG1γ production, observed only in mice vaccinated with 50 µg, while Fig. 3F demonstrates a greater presence of IgG2b antibodies after the booster dose in both groups. The results we have obtained demonstrate the superiority of the IgG2b response compared to the IgG1 response, which is in line with findings from other studies utilizing bacteriophage VLPs[58].

After the evaluation of the humoral immune response, we assessed cellular immunity, focusing on the induction of specific T cells, particularly Th1 cells. To achieve this, we performed ICCS to measure the production of IFNγ, a cytokine known for its involvement in immune regulation and antiviral effects. In Fig. 3 G-J, it is evident that the vaccine effectively stimulated T cells, specifically $CD4^+$ T cells in the spleen (Fig. 3 G-H) and lymph nodes (Fig. 3 I-J), to produce IFNγ, regardless of the vaccine formulation used (20–50 µg).

Neutralization capacity of antibodies from vaccinated mice

In this study, we employed the cPass SARS-CoV-2 Neutralization Antibody Detection Kit (GenScript, USA Ref. L00847) to evaluate the capacity of hyperimmune serum samples from mice immunized with 20 µg and 50 µg of the vaccine, 14 days after the booster dose. Figure 4 A demonstrates that both vaccine doses (20 µg and 50 µg) elicit the production of neutralizing antibodies (nAbs) that effectively recognize and inhibit the binding of RBD to hACE2, with percentages of 90.5% and 92.3%, respectively. These percentages were compared to the controls provided by the kit as well as PBS, RBD, and QβVLPs hyperimmune serum. Additionally, to determine the presence of nAbs against SARS-CoV-2, we conducted an in vitro microneutralization assay using the Vero E6 cell line, which expresses the ACE2 receptor on its surface. The results demonstrated that hyperimmune sera from mice immunized with 50 µg and 20 µg of the QβVLPs - RBD vaccine were capable of neutralizing the P.1 SARS-CoV-2 strain (Gamma variant) compared to the control groups (Fig. 4 B). The group of mice immunized with 50 µg was particularly effective, neutralizing 100% of the virus in dilutions ranging from 1/20 to 1/60, and 80% in dilutions from 1/540 to 1/1600. A colorimetric reading based on optical density values accurately assessed the ratio of infected cells to non-infected cells, facilitating the processing of a large number of samples within 72 h.

Challenges and assessment of clinical signs, viral load, inflammation, and histopathology

The data presented above provide insights into the immune responses induced by two doses of the vaccine formulations (20 µg and 50 µg). This encompasses the generation of both humoral and cellular immune responses, along with the production of neutralizing antibodies. Although the vaccine formulation with 50 µg

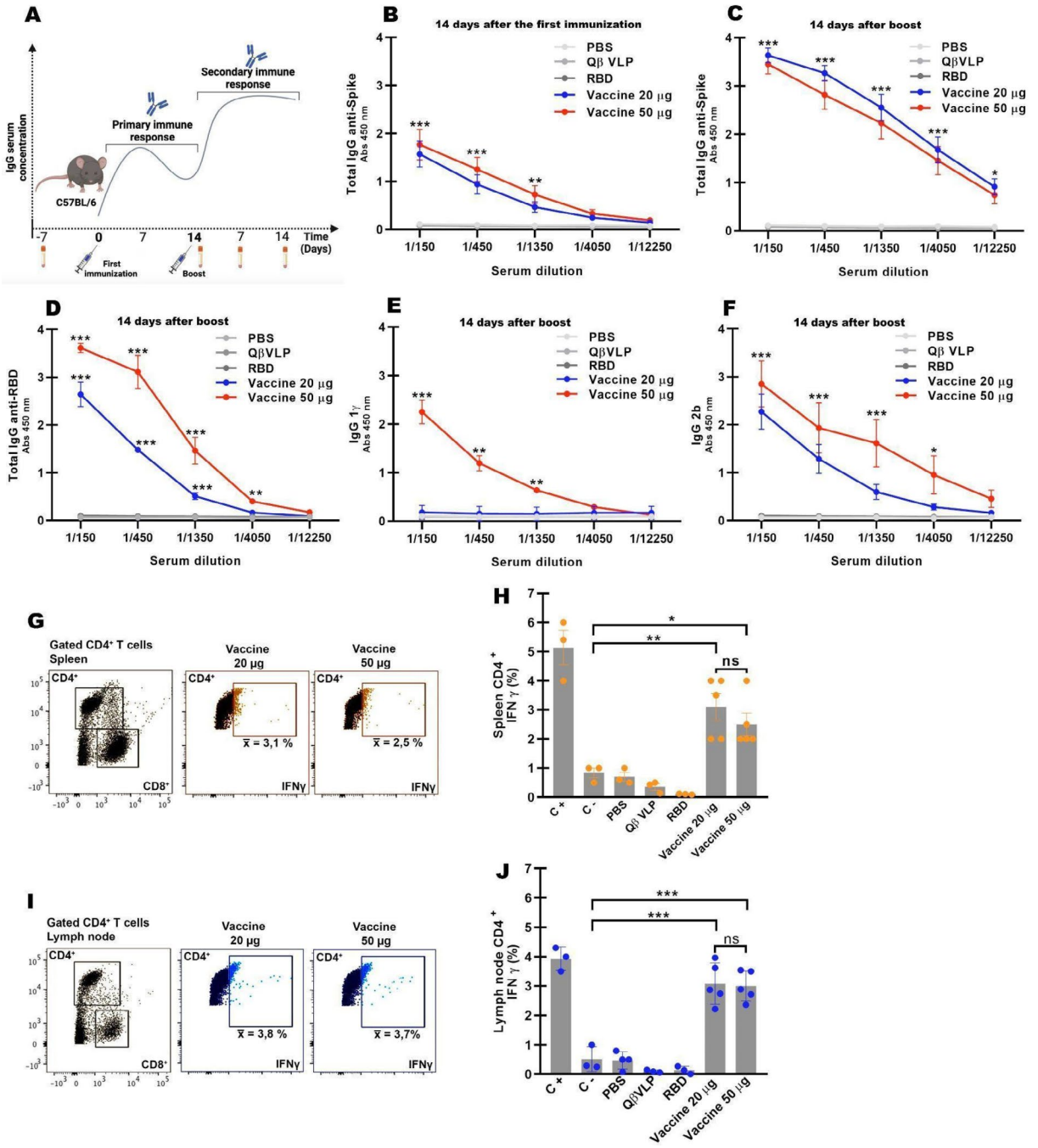

Fig. 3. Immunological assessment of the vaccine formulation. **(A)** - Schedule of mouse (C57BL/6) immunization in two doses (day 0 and boost) and serum collection after immunizations. **(B-C)** Profile of total IgG anti-Spike production of serum collected 14 days after first and second immunization with 20 µg, 50 µg, and controls (PBS, QβVLPs, and RBD), respectively. **(D)** Total IgG anti-RBD production of serum collected 14 days after boost with 20 µg, 50 µg, and controls. **(E-F)** Production of IgG2b and IgG1γ anti-Spike present in the serum collected 14 days after the second immunization with 20 µg, 50 µg, and controls. ELISA results show an average of three experiments ± SEM. *** $P \leq 0.001$ compared with PBS, RBD, and QβVLPs controls. The results show an average of three experiments ± SEM. *** $P \leq 0.001$ compared with PBS, RBD, and QβVLPs controls. **(G-J)** Profile of intracellular IFNγ production by lymphocytes of the mice immunized with QβVLPs-RBD vaccine analyzed by flux cytometry. **(G-H)** Detection of IFNγ production in CD4+ T lymphocytes from the spleen extracted from mice immunized with the QβVLPs-RBD vaccine (20 µg and 50 µg) RBD, QβVLPs or PBS and subsequently stimulated with the Spike recombinant protein. **(I-J)** Detection of IFNγ production in T lymphocytes CD4+ from cervical lymph nodes extracted from mice immunized with the QβVLPs-RBD vaccine (20 µg and 50 µg), RBD, QβVLPs or PBS and subsequently stimulated with the Spike recombinant protein. Negative control: PBS. Positive control: PMA + Ionomycin. The results show an average of three experiments ± SEM. *** $P \leq 0.001$ compared with negative control (C-).

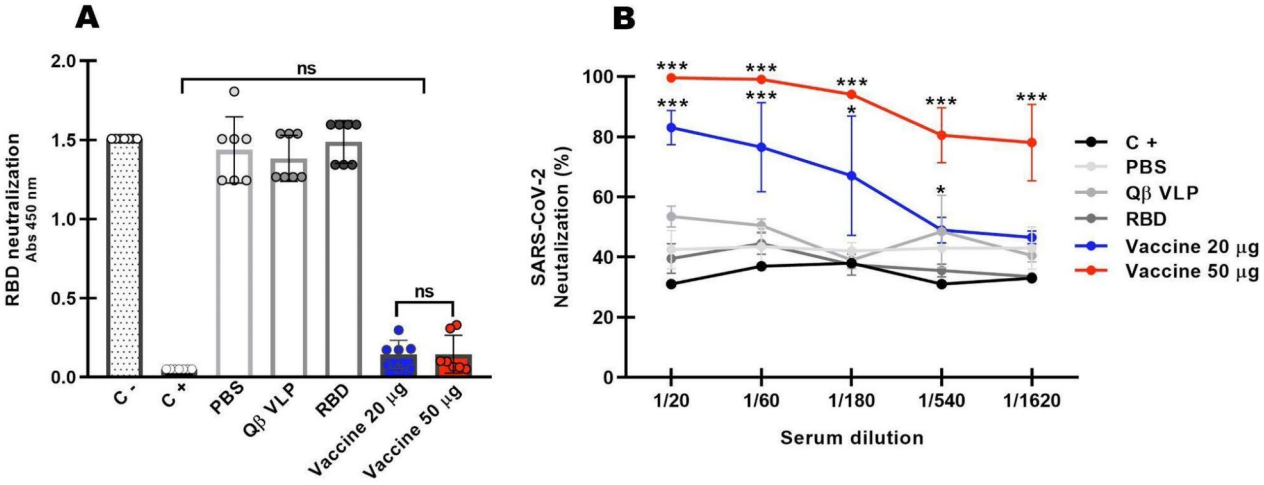

Fig. 4. Neutralizing antibodies assay. **(A)** The samples collected from vaccinated and control group of mice were diluted 1:10 and incubated with RBD conjugated with HRP and after were added in the 96 wells plate previously coating with ACE2, as described on the Kit cPass SARS-CoV-2 Neutralization Antibody Detection Kit (GenScript, EUA Ref. L00847). Negative (without antibody) and positive controls (positive neutralizing antibody) are purchased from the kit. The average ± standard errors are shown, with significance levels $^{***}P \leq 0.001$ compared with positive control and PBS, RBD, and QβVLPs controls. **(B)** In vitro microneutralization assay. P1. SARS-CoV-2 were incubated with hyperimmune serum samples of 14 days after boost of the QβVLPs-RBD vaccine (20 µg and 50 µg), and controls (RBD, QβVLPs or PBS in a 1/3 dilution ratio. After, Vero E6 monolayer sub cultivated in 96 well plates were incubated with P.1 SARS-CoV-2 + hyperimmune sera samples for 72 h at 37 ºC in 5% CO_2. After this, it was added and the absorbance was measured in a plate reader in the range of 620 nm. The average ± standard errors are shown, with significance levels $^{***}P \leq 0.001$ compared with positive control and PBS, RBD, and QβVLPs controls.

exhibited slightly enhanced immunity, there was no statistically significant difference compared to the 20 µg formulation. From the available data, it can be inferred that both vaccine formulations (20 µg and 50 µg) elicited comparable immune responses in vaccinated animals. Therefore, we immunized groups of B6.Cg-Tg(K18-ACE2)2Prlmn mice with the most potent vaccine formulations (20 µg and 50 µg), alongside control groups (PBS, RBD, and QβVLPs), following the established immunization schedule. Subsequently, these mice were challenged with 10^6 virus particles of P.1 SARS-CoV-2 and monitored for seven days to evaluate clinical signs, behaviors, survival rates, and weight fluctuations (Fig. 5 A-B). Remarkably, all mice immunized with either 20–50 µg of the vaccine survived the challenge, whereas all control mice administered PBS, RBD, or QβVLPs alone succumbed to infection (Fig. 5 A, purple line with star). The control groups, comprising unvaccinated animals, were unable to withstand the final virus exposure.

The PBS and QβVLPs groups exhibited weight loss exceeding 20%, while the RBD group experienced weight loss exceeding 10%. Additionally, control groups displayed other clinical signs of disease, such as impaired mobility, ruffled fur, and hunching. Conversely, the group vaccinated with 50 µg of QβVLPs-RBD maintained a stable body weight throughout the experiment and showed no clinical signs. In the group vaccinated with 20 µg of QβVLPs-RBD, two mice experienced a 10% reduction in body weight, but no clinical signs were observed. It is crucial to emphasize that the safety assessment was conducted throughout the period when animals were immunized for the immune response tests. Observations revealed that the mice did not exhibit behavioral changes indicative of discomfort or pain, such as weight loss, dehydration, piloerection, hunched posture, social isolation, or vocalizations upon handling. Furthermore, as detailed in the results of the SARS-CoV-2 challenge tests (Fig. 5), the immunized animals were closely monitored for vital signs. These signs remained within normal ranges, with no observed weight loss, and all animals survived until the conclusion of the experiment. Furthermore, lung samples from mice vaccinated with 20 µg and 50 µg of QβVLPs-RBD vaccine exhibited a significantly lower viral load of SARS-CoV-2 compared to non-immunized animals (Fig. 5 C). These results indicate that the 50 µg QβVLPs-RBD vaccine was more effective in reducing viral load compared to the 20 µg QβVLPs-RBD vaccine.

At the conclusion of the experiment, the B6.Cg-Tg(K18-ACE2)2Prlmn immunized and control groups of mice were euthanized after seven days of being challenged. Lung necropsies were performed to assess the outcomes. Figure 6 illustrates the findings, comparing uninfected control animals (Fig. 6 A, B, and C) with infected control groups (PBS, RBD, and QβVLPs) depicted in Fig. 6 D-I.

Gross lung lesions and pulmonary pathology consistent with interstitial pneumonia were observed in the infected control groups, characterized by type II pneumocyte hyperplasia (Fig. 6H). Additionally, there was evidence of alveolar and perivascular inflammation, consisting of lymphocytes, macrophages, and neutrophils (Fig. 6 E and I). Variable amounts of alveolar fibrin, edema, and hemorrhage were present (Fig. 6 F), along with frequent syncytial and single cell necrosis (Fig. 6 G).

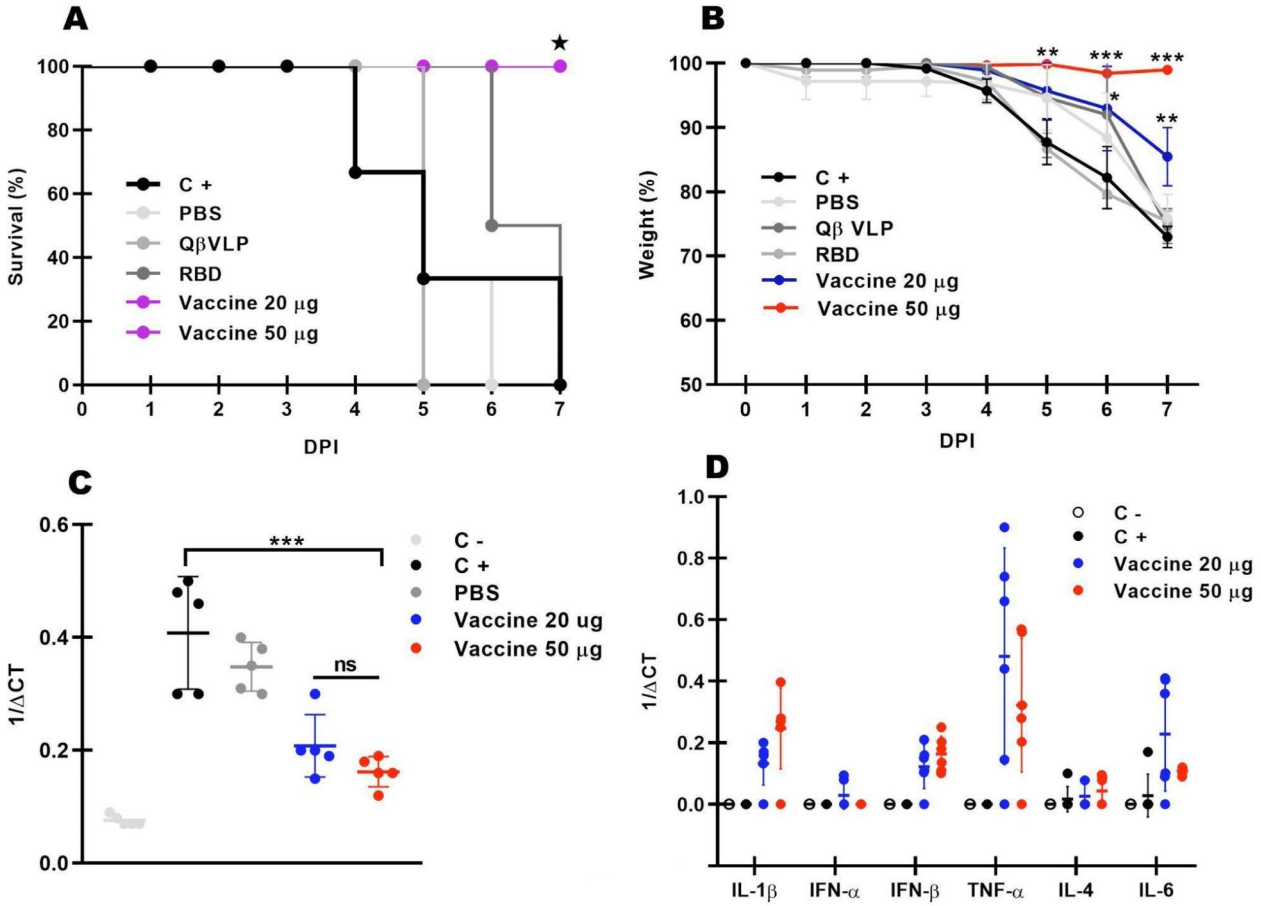

Fig. 5. Challenge with SARS-CoV-2 and assessment of clinical signs and viral. Two-dose immunization (20 μg and 50 μg) was able to protect K18-hACE-2 animals (model for severe COVID-19 from mortality, weight loss and other clinical signs of the disease such as motility, bristling hair and hunchback position. **(A)** Survival (%) after 7 days post infection (DPI); (in purple and highlighted with a star the survival rate of animals vaccinated with 20 μg and 50 μg of QβVLPs-RBD). **(B)** Loss weight (%) after 7 DPI. Mice immunized with 50 μg QβVLPs-RBD showed no significant weight loss while non immunized had more than 20% of body weight loss, in addition to showing the clinical symptoms of the disease. The average ± standard errors are shown, with significance levels $^{***}P \leq 0.001$ compared with positive control (C+). **(C)** Viral quantitative measurements by qRT-PCR showed a significantly lower viral load of SARS-CoV-2 in the lungs of mice vaccinated with two-dose immunization (20 μg and 50 μg) in comparison to non-immunized animals The average ± standard errors are shown, with significance levels $^{***}P \leq 0.001$ compared with positive control (C+). **(D)** Cytokine profile expression measurements by qRT-PCR. Negative Control (C-): Samples from animals that were neither vaccinated nr exposed to the virus (naive animals). Positive Control (C+): Samples from animals that, while not vaccinated, were exposed to the virus.

The immunized animals that received two doses of 20 μg QβVLPs-RBD also displayed interstitial pneumonia characterized by type II pneumocyte hyperplasia and alveolar fibrin deposition (Fig. 6 J-L), but to a lesser extent when compared to the infected control groups. Furthermore, this group (20 μg) exhibited lower perivascular inflammation (Fig. 6 J) than the infected control groups.

The lungs of the animals that received two doses of 50 μg QβVLPs-RBD closely resembled those of the uninfected control groups, and showed significantly less damage compared to the infected control groups, as well as in comparison to the vaccinated animals receiving 20 μg. Figure 6 M indicates minimal perivascular inflammation of polymorphonuclear cells, in contrast to Fig. 6 D-E, while the alveoli exhibited a similar appearance to the non-infected control (Fig. 5 N); the type II pneumocyte cells displayed normal morphology (Fig. 6 O).

Discussion

Advances and challenges in vaccine technology: focus on VLPs

Advancements in vaccine technology are crucial for addressing global health challenges. Traditional licensed vaccines often rely on adjuvants to stimulate Th1-helper cell responses. However, the limited availability and high

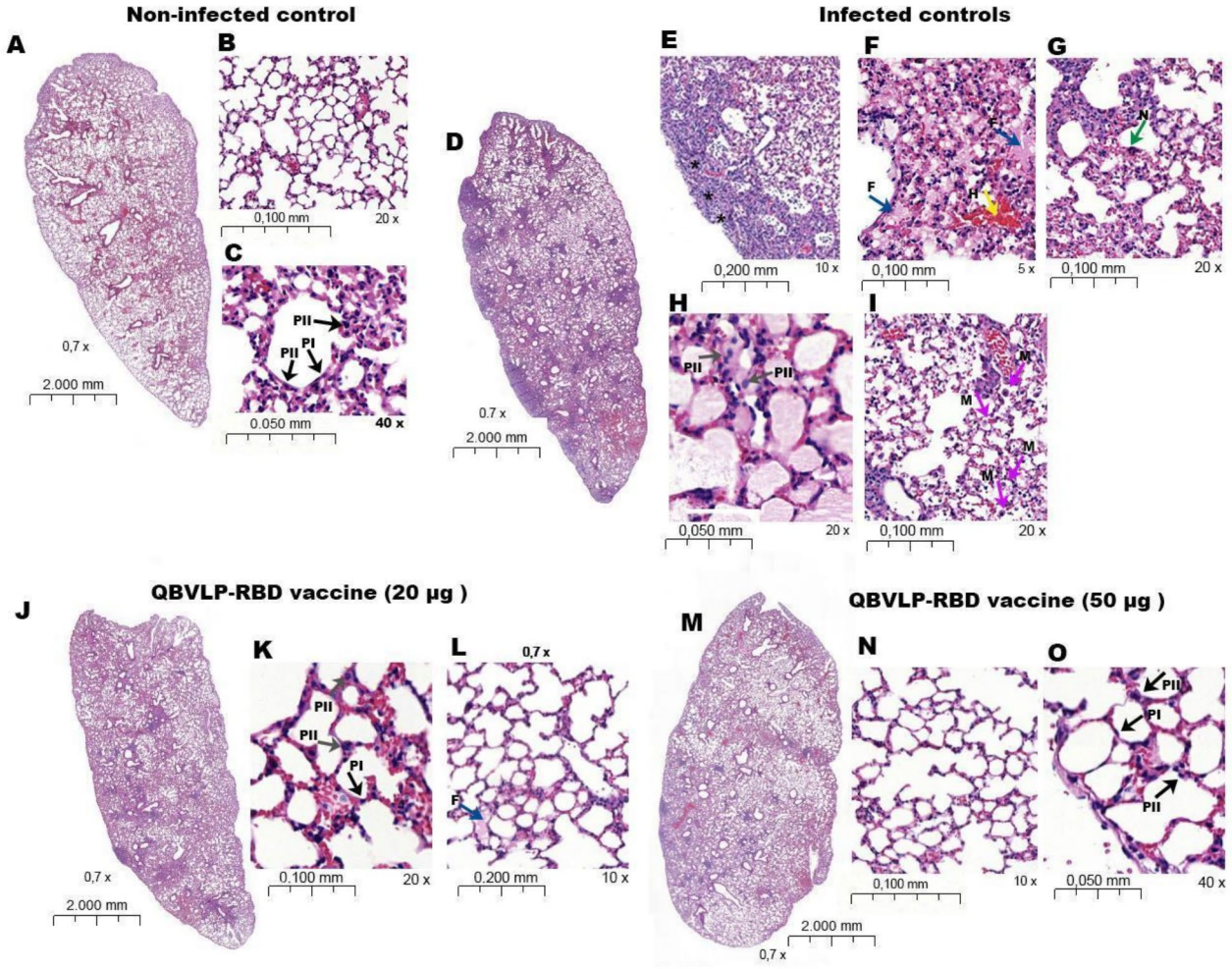

Fig. 6. Lung histopathological analysis of immunized B6.Cg-Tg(K18-ACE2)2Prlmn animals challenged with SARS-CoV-2. **(A-C)** Lung of non-infected animals. **(A)** Panoramic lung vision. **(B)** Lung parenchyma with normal appearance. **(C)** Type I and II pneumocytes with normal morphology (arrow black PI and arrow black PII). **(D-I)** Lung of the infected controls animals previously immunized with PBS, RBD, and QβVLPs. **(D)** Panoramic lung vision. **(E)** Perivascular inflammation (asterisk). **(F)** Alveolar fibrin and hemorrhage (blue F and yellow H arrows, respectively). **(G)** Syncytial and single cell necrosis (green N arrow). **(H)** Type II pneumocyte hyperplasia (gray PII arrows). **(I)** Macrophages (pink M arrows). **(J-L)** Lung os the infected controls animals previously immunized with QβVLPs-RBD vaccine (20 µg). **(J)** Panoramic lung vision. **(K)** Type II pneumocyte hyperplasia (gray PII arrows). **(L)** Alveolar fibrin (blue F arrow). **(M-O)** Lung os the infected controls animals previously immunized with QβVLPs-RBD vaccine (50 µg). **(M)** Panoramic lung vision. **(N)** Lung parenchyma with normal appearance. **(O)** Type I and II pneumocytes with normal morphology (arrow black PI and arrow black PII). The 4 µm thick sections were stained with hematoxylin and eosin and images were captured with Slide Digitizer – 3D Histech scanner and analyzed in Download CaseViewer 2.4, 64-bit version (3D- Histotech, Hungary - https://www.3dhistech.com/solutions/caseviewer/).

costs of these adjuvants present significant obstacles to developing universal, low-cost vaccination strategies. The advent of mRNA vaccine technology represents a significant advancement in the field of immunization, with the potential to surpass traditional vaccine formulations. Unlike conventional vaccines and subunit vaccines, which often require the addition of adjuvants to enhance immune responses, mRNA vaccines can stimulate robust immune responses without these additives. However, despite their transformative potential, mRNA vaccines face considerable challenges related to the stability and delivery of mRNA, and the stringent storage requirements of these vaccines pose logistical difficulties, particularly in resource-limited and remote settings. Current research is concentrated on improving mRNA translation efficiency and safeguarding mRNA from degradation, with lipid nanoparticles emerging as a pivotal component in these enhancements[35–39]. Nevertheless, the dependence on large pharmaceutical companies for these vaccine components highlights the urgent need for more accessible vaccine technologies, especially for neglected diseases.

Viral vector-based vaccines present a promising alternative, with proven effectiveness and versatility. Recent advancements in this technology include genetic modifications designed to enhance both the efficiency and

safety of these vaccines. Additionally, the development of heterologous vaccination strategies has been pivotal in improving overall efficacy and durability. Despite these advancements, a potential decline in vaccine efficacy over time due to the immune system's response to the viral vector remains a challenge. To address this, heterologous vaccine boosters are employed to sustain long-term immunological protection by diversifying the immune response and counteracting the diminishing effectiveness[40–42].

Having access to diverse and functional vaccine platforms is essential from both logistical and immunological perspectives. Such diversity enables customization based on local needs and allows for strategies to address reduced vaccine efficacy following multiple doses, particularly when using heterologous booster approaches. Moreover, amidst the collective suffering of human tragedies and economic losses caused by pandemics, it has become increasingly clear that prioritizing the development of locally produced vaccine platforms is a vital component of pandemic preparedness. This involves creating a range of vaccines using various technologies that can be adapted to other pathogens with pandemic potential[43–46].

In this context, our study presents a promising vaccine formulation utilizing QβVLPs. These VLPs are nanoparticles with an icosahedral capsid structure, consisting of 180 subunits derived from the coat protein of the Qβ bacteriophage[47]. This structure allows the VLPs to retain a substantial amount of bacterial RNA within their core. Non-viral RNA is incorporated into QβVLPs in vivo through an RNA hairpin derived from Qβ RNA, which has a strong affinity for the coat protein. During VLPs assembly, the coat protein interacts with the RNA hairpin via the RNA backbone, and specific sequence interactions[48,49]. Bacterial RNA plays a crucial role in activating the innate immune system by acting as an agonist for Toll-like receptors (TLR) 7 and 8, which are present in the endosomes of certain immune cells. This property has demonstrated significant immunogenic potential in vaccines formulated with QβVLPs, as evidenced by the early transcriptional responses in APCs and the subsequent T cell response following immunization[15]. The particle size is critical for immune activation, as these particles can efficiently drain into the lymphatic system through lymphatic vessel pores, facilitating recognition by APCs in lymphoid organs and prompt antigen presentation to follicular T cells. This contributes to a comprehensive activation of the immune system, from innate to adaptive, enhancing the efficiency of humoral immunity and antibody production dependent on T cells[15,50].

It is crucial to highlight that numerous studies have demonstrated promising results with QβVLPs in both preclinical and clinical settings. Research has explored their applications in infectious diseases, as discussed here, as well as in chronic conditions. Notably, QβVLPs have been investigated for treatments involving Angiotensin-II peptide conjugated to QβVLPs for hypertension, therapeutic interventions for nicotine dependence, and vaccines targeting oligomeric alpha-synuclein[30,51,52].

Engineering VLPs to display a variety of antigens is complex and achieving high-density antigen display is essential to maximize their immunogenic potential. Various methods have been developed to utilize VLPs as effective scaffolds for antigen presentation, taking advantage of their versatility to accommodate different antigens in terms of composition, size, and structure. One method involves inserting foreign antigens into viral structural proteins for display on the VLPs surface[49]. However, this can disrupt VLP assembly. To address this, preformed VLPs can serve as scaffolds for antigen attachment via conjugation techniques. Post-production modifications can use natural conjugation sites or engineered functionalities. For example, bacteriophage QβVLPs feature amino groups on exposed lysines, ideal for linking to cysteine-containing antigens with bifunctional cross-linkers. This method avoids disrupting VLPs assembly and is suitable for GMP production, with several Qβ-based vaccines already tested in clinical trials.

Despite significant advancements, accurately characterizing vaccine conjugation continues to present challenges. Although SDS-PAGE is a widely used method for this purpose, it may not always yield clear results. To address these limitations, complementary techniques such as TEM are employed. As demonstrated in our results, TEM provides valuable insights into the morphology of VLPs and their conjugates, offering a more comprehensive understanding of their structural characteristics. Additionally, techniques such as matrix-assisted laser desorption ionization time-of-flight mass spectrometry (MALDI-TOF MS), liquid chromatography–mass spectrometry (LC–MS), reverse-phase high-performance liquid chromatography (RP-HPLC), cryo-electron microscopy (Cryo-EM), atomic force microscopy (AFM), high-performance size exclusion chromatography (HPSEC), and surface plasmon resonance (SPR)[53] can further enhance the analysis of vaccine conjugation.

Maximizing the production yield of nanoparticles is a crucial objective in vaccine development due to its significant impact on vaccine cost. Utilizing *E. coli* offers several advantages, particularly when proteins are synthesized in the soluble fraction with proper folding, as demonstrated in our production strategy. *E. coli* has previously shown a strong safety profile and high efficacy[54], and it simplifies scaling up production through bioreactor technology.

Comprehensive evaluation of vaccine efficacy: immune response, protection, and lung pathology

Considering the emergence of new SARS-CoV-2 variants of concern, which have shown partial evasion of immune responses from previous vaccinations or natural infections, there is an urgent need to advance and adapt vaccine technologies for optimal protection, safety, and affordability[55,56]. Vaccine strategies that have demonstrated effectiveness in both preclinical and clinical studies, such as those based on VLPs, offer promising alternatives. For example, VLPs-based vaccines displaying the RBD of the SARS-CoV-2 spike protein and modular capsid VLPs have shown significant potential[57,58]. Currently, several recombinant spike protein RBD vaccines, produced in various cell lines including Pichia pastoris, Chinese hamster ovary (CHO) cells, and Expi 293T cells, have received regulatory approval. These vaccines often include adjuvants like aluminum hydroxide and/or AS03 to enhance immunogenicity[59–65]. Furthermore, 55 protein subunit vaccines are currently in preclinical evaluation[66].

Our study focuses on a VLPs-based vaccine designed to deliver the spike protein's RBD antigen, with the objective of stimulating cellular immune components without the need for adjuvants. This approach aims to improve the vaccine's applicability and affordability. We have achieved exceptional reproducibility in our vaccine formulations by modifying QβVLPs nanoparticles with SMPH bifunctional cross-linkers and antigen modifications using SATA and hydroxylamine hydrochloride[26–29].

Incorporation of bacterial RNA during QβVLPs assembly enhances their immunogenicity by engaging pattern recognition receptors such as TLR[67]. This process has been linked to increased IgG2b and IgG2c levels and reduced IgG1, indicating a robust Th1 response. The production of IgG antibodies dependent on T helper cell activity, is closely linked to the vaccine's neutralizing capacity and overall effectiveness. Specifically, the Th1 cytokine IFN-γ promotes the production of IgG2, while the Th2 cytokine IL-4 drives the expression of IgG1[68–71]. Our results indicate that the vaccine formulation elicits a strong immune response independently of additional adjuvants, suggesting its potential for broad applicability. The antibodies generated are not only neutralizing but also provide protective immunity.

Following the assessment of humoral immunity, we evaluated cellular immunity, particularly the induction of specific T cells, with an emphasis on Th1 cells. This evaluation is critical for vaccine development. Our findings demonstrate that the vaccine formulation effectively stimulates both adaptive cellular and humoral immune responses, distinguishing it from other vaccines that typically require such adjuvants[67]. VLPs effectively present antigens to T cells through dendritic cells by utilizing MHC molecules. This antigen presentation mechanism is consistent with the performance observed in other VLP-based vaccines targeting a range of viruses, such as Zika virus (ZIKV), Ebola virus, Chikungunya virus (CHIKV), Dengue virus (DENV), influenza, and SARS-CoV-2[68–75].

In vivo challenge tests using genetically modified C57BL/6 mice expressing human ACE2 provide a highly relevant model for evaluating the efficacy of vaccines against SARS-CoV-2. This model closely mimics human infection, offering valuable insights into the vaccine's performance in conditions that resemble actual human disease[76]. Our study demonstrated that the vaccine formulations tested conferred significant protection, as evidenced by reduced viral loads, diminished lung pathology, and improved overall health outcomes in the vaccinated mice compared to controls. These results underscore the vaccine's ability to not only elicit robust immune responses but also to protect effectively against infection and mitigate disease severity.

Understanding the nuances of the immune response, particularly the role of pro-inflammatory cytokines, is essential for assessing vaccine efficacy. Our findings revealed a significant increase in the production of IFN-γ by CD4 + T cells in vaccinated animals compared to controls, highlighting the vaccine's effectiveness in inducing a robust immune response. The levels of key cytokines such as IL-1β, IL-6, and TNF-α, which are critical for antiviral defenses, exhibited a strong correlation with disease severity. Additionally, IL-4 plays a crucial role in modulating the immune response. The QβVLPs-based vaccines effectively engage both humoral and cellular immune mechanisms, facilitating efficient antigen presentation and cytokine release. This dual activation promotes a comprehensive and enduring immune response, as demonstrated by the observed immune profiles[77–80].

Conclusion

This study presents a promising advancement in vaccine technology through the development of a novel VLPs-based vaccine utilizing QβVLPs chemically modified with receptor-RBD antigens. Our findings demonstrate that this vaccine formulation induces robust humoral and cellular immune responses, eliciting specific binding and neutralizing antibodies against SARS-CoV-2, and effectively protects against the virus in murine models without requiring additional adjuvants.

The QβVLP-based vaccine offers significant advantages over traditional vaccine platforms, including a favorable safety profile and the potential for adaptability to VOCs. Its effectiveness in inducing immunity without the need for adjuvants addresses the limitations associated with current vaccine technologies, such as the need for costly adjuvants and stringent storage conditions.

Future research will be essential to investigate the long-term durability of the immune response and evaluate the vaccine's efficacy in diverse populations and under varying conditions. Additionally, exploring strategies to optimize vaccine dosage and vaccination schedules, particularly in the context of heterologous boosting, will be crucial for advancing this technology toward clinical application.

In summary, the QβVLP-based vaccine represents a significant step forward in vaccine development, with the potential to contribute effectively to global health initiatives. Continued research and development are needed to further refine this approach and ensure its broad applicability and sustained impact on public health.

Data availability

All data, code, and materials used in the analysis are available to any researcher for purposes of reproducing or extending the analysis. The sequence of the Spike protein produced (containing amino acids 1-1208 of the ectodomain, followed by the tail) is a sequence published by Wrapp et al. (2020 - Science, doi: 10.1126/science.abb2507). Requests for the materials should be submitted to the corresponding author. All data needed to evaluate the conclusions in the paper are present in the paper.

Received: 19 June 2024; Accepted: 10 October 2024
Published online: 16 October 2024

References

1. Kumar, A. et al. SARS-CoV-2-specific virulence factors in COVID-19. *J. Med. Virol.* **93** (3), 1343–1350. https://doi.org/10.1002/jmv.26615 (2021). Epub 2020 Nov 1. PMID: 33085084.
2. World Health Organization. WHO Coronavirus (COVID-19) Dashboard. https://covid19.who.int/
3. DeGrace, M. M. et al. Defining the risk of SARS-CoV-2 variants on immune protection. *Nature*. **605**, 640–652 (2022).
4. Prates-Syed, W. A. et al. VLP-Based COVID-19 vaccines: an adaptable technology against the threat of New variants. *Vaccines (Basel)*. **9** (12), 1409. https://doi.org/10.3390/vaccines9121409 (2021). PMID: 34960155; PMCID: PMC8708688.
5. Chirico, F., da Silva, J. A. T., Tsigaris, P. & Sharun, K. Safety & effectiveness of COVID-19 vaccines: a narrative review. *Indian J. Med. Res.* **155**, 91–104 (2022).
6. Jackson, C. B., Farzan, M., Chen, B. & Choe, H. Mechanisms of SARS-CoV-2 entry into cells. *Nat. Rev. Mol. Cell. Biol.* **23**, 3–20 (2022).
7. Min, L. & Sun, Q. Antibodies and vaccines target RBD of SARS-CoV-2. *Front. Mol. Biosci.* **8**, 671633 (2021).
8. Premkumar, L. et al. The receptor binding domain of the viral spike protein is an immunodominant and highly specific target of antibodies in SARS-CoV-2 patients. *Sci. Immunol.* **5** (48), eabc8413. https://doi.org/10.1126/sciimmunol.abc8413 (2020). PMID: 32527802; PMCID: PMC7292505.
9. Pollet, J., Chen, W. H. & Strych, U. Recombinant protein vaccines, a proven approach against coronavirus pandemics. *Adv. Drug Deliv Rev.* **170**, 71–82. https://doi.org/10.1016/j.addr.2021.01.001 (2021). Epub 2021 Jan 7. PMID: 33421475; PMCID: PMC7788321.
10. Pulendran, B. S., Arunachalam, P. & O'Hagan, D. T. Emerging concepts in the science of vaccine adjuvants. *Nat. Rev. Drug Discov.* **20**, 454–475 (2021).
11. Schijns, V. et al. Modulation of immune responses using adjuvants to facilitate therapeutic vaccination. *Immunol. Rev.* **296** (1), 169–190. https://doi.org/10.1111/imr.12889 (2020). Epub 2020 Jun 28. PMID: 32594569; PMCID: PMC7497245.
12. Zhang, Y. N., Auclair, S. & Zhu, J. Virus-like nanoparticle vaccines for inducing long-lasting immunity against infectious diseases. *Natl. Sci. Rev.* **11** (4), nwae032. https://doi.org/10.1093/nsr/nwae032 (2024). PMID: 38440215; PMCID: PMC10911813.
13. Gao, X. et al. Nanovaccines for advancing long-lasting immunity against Infectious diseases. *ACS Nano*. **17** (24), 24514–24538. https://doi.org/10.1021/acsnano.3c07741 (2023). Epub 2023 Dec 6. PMID: 38055649.
14. Kang, S. M. et al. Induction of long-term protective immune responses by influenza H5N1 virus-like particles. *PLoS One*. **4** (3), e4667. https://doi.org/10.1371/journal.pone.0004667 (2009). Epub 2009 Mar 2. PMID: 19252744; PMCID: PMC2646145.).
15. Mohsen, M. O. L., Zha, Cabral-Miranda, G. & Bachmann, M. F. Major findings and recent advances in virus-like particle (VLP)-based vaccines. *Semin Immunol.* **34**, 123–132 (2017).
16. Gupta, R. et al. Platforms, advances, and technical challenges in virus-like particles-based vaccines. *Front. Immunol.* **14**, 1123805. https://doi.org/10.3389/fimmu.2023.1123805 (2023). PMID: 36845125; PMCID: PMC9947793.
17. Tariq, H., Batool, S., Asif, S., Ali, M. & Abbasi, B. H. Virus-like particles: Revolutionary platforms for developing vaccines against emerging Infectious diseases. *Front. Microbiol.* **12**, 790121. https://doi.org/10.3389/fmicb.2021.790121 (2022). PMID: 35046918; PMCID: PMC8761975.
18. Dhawan, M., Saied, A. R. A. & Sharma, M. Virus-like particles (VLPs)-based vaccines against COVID-19: where do we stand amid the ongoing evolution of SARS-CoV-2? *Health Sci. Rev.* **9**, 100127. https://doi.org/10.1016/j.hsr.2023.100127 (2023).
19. Mohsen, M. O. et al. Delivering adjuvants and antigens in separate nanoparticles eliminates the need of physical linkage for effective vaccination. *J. Controlled Release 2017 March* **251**: 92–100. https://doi.org/10.1016/j.jconrel.2017.02.031
20. Qian, C. et al. Recent progress on the versatility of Virus-Like particles. *Vaccines (Basel)*. **8** (1), 139. https://doi.org/10.3390/vaccines8010139 (2020). PMID: 32244935; PMCID: PMC7157238.
21. Zhou, F. & Zhang, D. Recent advance in the development of tuberculosis vaccines in clinical trials and virus-like particle-based vaccine candidates. *Front. Immunol.* **14**, 1238649. https://doi.org/10.3389/fimmu.2023.1238649 (2023). PMID: 38022657; PMCID: PMC10652786.
22. Hadj Hassine, I., Ben, M., Almalki, M. & Gharbi, M. A. Virus-like particles as powerful vaccination strategy against human viruses. *Rev. Med. Virol.* **34** (1), e2498. https://doi.org/10.1002/rmv.2498 (2024). Epub 2023 Dec 20. PMID: 38116958.
23. Mazalovska, M. & Kouokam, J. C. Progress in the production of Virus-Like particles for vaccination against Hepatitis E Virus. *Viruses*. **12** (8), 826. https://doi.org/10.3390/v12080826 (2020). PMID: 32751441; PMCID: PMC7472025.
24. Wang, D. et al. Rational design of a multi-valent human papillomavirus vaccine by capsomere-hybrid co-assembly of virus-like particles. *Nat. Commun.* **11** (1), 2841. https://doi.org/10.1038/s41467-020-16639-1 (2020). PMID: 32503989; PMCID: PMC7275066.
25. Bahar, M. W. et al. Mammalian expression of virus-like particles as a proof of principle for next generation polio vaccines. *NPJ Vaccines*. **6** (1), 5. https://doi.org/10.1038/s41541-020-00267-3 (2021). PMID: 33420068; PMCID: PMC7794334.
26. Cabral-Miranda, G. et al. M. DOPS Adjuvant Confers Enhanced Protection against Malaria for VLP-TRAP Based Vaccines. *Diseases* ;**6**(4):107. doi: https://doi.org/10.3390/diseases6040107. (2018). PMID: 30469323; PMCID: PMC6313579.
27. Cabral-Miranda, G. et al. Microcrystalline Tyrosine (MCT®): a Depot Adjuvant in Licensed Allergy Immunotherapy offers New opportunities in Malaria. *Vaccines (Basel)*. **5** (4), 32. https://doi.org/10.3390/vaccines5040032 (2017). PMID: 28953265; PMCID: PMC5748599.
28. Cabral-Miranda, G. et al. Virus-like particle (VLP) plus Microcrystalline Tyrosine (MCT) adjuvants enhance vaccine efficacy improving T and B cell immunogenicity and protection against Plasmodium berghei/vivax. *Vaccines (Basel)*. **5** (2), 10. https://doi.org/10.3390/vaccines5020010 (2017). PMID: 28468322; PMCID: PMC5492007.
29. Roesti, E. S. et al. Vaccination against Amyloidogenic Aggregates in pancreatic islets prevents development of type 2 diabetes Mellitus. *Vaccines (Basel)*. **8** (1), 116. https://doi.org/10.3390/vaccines8010116 (2020). PMID: 32131431; PMCID: PMC7157615.
30. Doucet, M. et al. Preclinical development of a vaccine against oligomeric alpha-synuclein based on virus-like particles. *PLoS One*. **12** (8), e0181844. https://doi.org/10.1371/journal.pone.0181844 (2017). PMID: 28797124; PMCID: PMC5552317.
31. Vanderheiden, A. et al. Development of a Rapid Focus Reduction Neutralization Test Assay for Measuring SARS-CoV-2 neutralizing antibodies. *Curr. Protoc. Immunol.* **131** (1), e116. https://doi.org/10.1002/cpim.116 (2020). PMID: 33215858; PMCID: PMC7864545.
32. Martino, M. L., Crooke, S. N., Manchester, M. & Finn, M. G. Single-point mutations in Qβ Virus-like particles change binding to cells. *Biomacromolecules*. **22** (8), 3332–3341. https://doi.org/10.1021/acs.biomac.1c00443 (2021). Epub 2021 Jul 12. PMID: 34251176; PMCID: PMC9068229.
33. Sungsuwan, S. et al. Structure guided design of bacteriophage Qβ mutants as Next Generation Carriers for Conjugate vaccines. *ACS Chem. Biol.* **17** (11), 3047–3058. https://doi.org/10.1021/acschembio.1c00906 (2022). Epub 2022 Feb 10. PMID: 35142488; PMCID: PMC9363528.
34. Brito, L. A. & Singh, M. Acceptable levels of endotoxin in vaccine formulations during preclinical research. J Pharm Sci. ;100(1):34 – 7. doi: (2011). https://doi.org/10.1002/jps.22267. PMID: 20575063.
35. Hou, X. et al. Lipid nanoparticles for mRNA delivery. *Nat. Rev. Mater.* **6**, 1078–1094. https://doi.org/10.1038/s41578-021-00358-0 (2021).
36. Huang, X. et al. The landscape of mRNA nanomedicine. *Nat. Med.* **28**, 2273–2287. https://doi.org/10.1038/s41591-022-02061-1 (2022).
37. Schoenmaker, L. et al. mRNA-lipid nanoparticle COVID-19 vaccines: structure and stability. *Int. J. Pharm.* **601**, 120586. https://doi.org/10.1016/j.ijpharm.2021.120586 (2021). Epub 2021 Apr 9. PMID: 33839230; PMCID: PMC8032477.

38. Li, X. et al. Nanoparticle technology for mRNA: delivery strategy, clinical application and developmental landscape. *Theranostics*. **14** (2), 738–760. https://doi.org/10.7150/thno.84291 (2024). PMID: 38169577; PMCID: PMC10758055.
39. Kon, E., Elia, U. & Peer, D. Principles for designing an optimal mRNA lipid nanoparticle vaccine. *Curr. Opin. Biotechnol.* **73**, 329–336. https://doi.org/10.1016/j.copbio.2021.09.016 (2022). Epub 2021 Oct 26. PMID: 34715546; PMCID: PMC8547895.
40. Wang, S. et al. Viral vectored vaccines: design, development, preventive and therapeutic applications in human diseases. *Signal. Transduct. Target. Ther.* **8** (1), 149. https://doi.org/10.1038/s41392-023-01408-5 (2023). PMID: 37029123; PMCID: PMC10081433.
41. Shirley, J. L., de Jong, Y. P., Terhorst, C. & Herzog, R. W. Immune responses to viral gene therapy vectors. *Mol. Ther.* **28** (3), 709–722. https://doi.org/10.1016/j.ymthe.2020.01.001 (2020). Epub 2020 Jan 10. PMID: 31968213; PMCID: PMC7054714.
42. Chan, Y. K. et al. Engineering adeno-associated viral vectors to evade innate immune and inflammatory responses. *Sci. Transl Med.* **13** (580), eabd3438. https://doi.org/10.1126/scitranslmed.abd3438 (2021). PMID: 33568518; PMCID: PMC8409505.
43. Syed, A. M. et al. Rapid assessment of SARS-CoV-2-evolved variants using virus-like particles. *Science*. **374** (6575), 1626–1632. https://doi.org/10.1126/science.abl6184 (2021). Epub 2021 Nov 4. PMID: 34735219; PMCID: PMC9005165.
44. Johnson, B. A. & Menachery, V. D. A new tool to probe SARS-CoV-2 variants. *Science*. **374** (6575), 1557–1558. https://doi.org/10.1126/science.abn3781 (2021). Epub 2021 Dec 23. PMID: 34941409.
45. Vuitika, L. et al. Vaccines against emerging and neglected infectious diseases: an overview. *Vaccines (Basel)*. **10** (9), 1385. https://doi.org/10.3390/vaccines10091385 (2022). PMID: 36146463; PMCID: PMC9503027.
46. Kaul, V. et al. Lessons learned from a global perspective of Coronavirus Disease-2019. *Clin. Chest Med.* **44** (2), 435–449 (2023). Epub 2022 Nov 24. PMID: 37085231; PMCID: PMC9684102.
47. Brown, S. D., Fiedler, J. D. & Finn, M. G. Assembly of hybrid bacteriophage Qbeta virus-like particles. *Biochemistry*. **48** (47), 11155–11157. https://doi.org/10.1021/bi901306 (2009). PMID: 19848414; PMCID: PMC2799296.
48. Chang, J. Y., Gorzelnik, K. V., Thongchol, J. & Zhang, J. Structural Assembly of Qβ Virion and its diverse forms of virus-like particles. *Viruses*. **14** (2), 225. https://doi.org/10.3390/v14020225 (2022). PMID: 35215818; PMCID: PMC8880383.
49. Frietze, K. M., Peabody, D. S. & Chackerian, B. Engineering virus-like particles as vaccine platforms. *Curr. Opin. Virol.* **18**, 44–49. https://doi.org/10.1016/j.coviro.2016.03.001 (2016). Epub 2016 Mar 29. PMID: 27039982; PMCID: PMC4983494.
50. Liao, W. et al. Characterization of T-Dependent and T-Independent B cell responses to a virus-like particle. *J. Immunol.* **198** (10), 3846–3856. https://doi.org/10.4049/jimmunol.1601852 (2017). Epub 2017 Apr 17. PMID: 28416599.
51. Ambühl, P. M. et al. A vaccine for hypertension based on virus-like particles: preclinical efficacy and phase I safety and immunogenicity. J Hypertens. ;25(1):63–72. doi: (2007). https://doi.org/10.1097/HJH.0b013e32800ff5d6. PMID: 17143175.
52. Maurer, P. et al. A therapeutic vaccine for nicotine dependence: preclinical efficacy, and Phase I safety and immunogenicity. Eur J Immunol. ;35(7):2031-40. doi: (2005). https://doi.org/10.1002/eji.200526285. PMID: 15971275.
53. Nooraei, S. et al. Virus-like particles: preparation, immunogenicity and their roles as nanovaccines and drug nanocarriers. *J. Nanobiotechnol.* **19** (1), 59. https://doi.org/10.1186/s12951-021-00806-7 (2021). PMID: 33632278; PMCID: PMC7905985.
54. Huang, X., Wang, X., Zhang, J., Xia, N. & Zhao, Q. Escherichia coli-derived virus-like particles in vaccine development. *NPJ Vaccines*. **2**, 3. https://doi.org/10.1038/s41541-017-0006-8 (2017). PMID: 29263864; PMCID: PMC5627247.
55. Markov, P. V. et al. The evolution of SARS-CoV-2. *Nat. Rev. Microbiol.* **21**, 361–379 (2023).
56. Nabel, K. G. et al. Structural basis for continued antibody evasion by the SARS-CoV-2 receptor binding domain. *Science*. **375** (6578), eabl6251. https://doi.org/10.1126/science.abl6251 (2022). Epub 2022 Jan 21. PMID: 34855508; PMCID: PMC9127715.
57. Smit, M. J. et al. First-in-human use of a modular capsid virus-like vaccine platform: an open-label, non-randomised, phase 1 clinical trial of the SARS-CoV-2 vaccine ABNCoV2. *Lancet Microbe*. **4** (3), e140–e148 (2023).
58. Fougeroux, C. et al. Capsid-like particles decorated with the SARS-CoV-2 receptor-binding domain elicit strong virus neutralization activity. *Nat. Commun.* **12** (1), 324 (2021).
59. Limonta-Fernández, M. et al. An engineered SARS-CoV-2 receptor-binding domain produced in Pichia pastoris as a candidate vaccine antigen. *N Biotechnol.* **72**, 11–21 (2022). Epub 2022 Aug 8. PMID: 35953030; PMCID: PMC9359770.
60. Hernández-Bernal, F. et al. Safety, tolerability, and immunogenicity of a SARS-CoV-2 recombinant spike RBD protein vaccine: a randomised, double-blind, placebo-controlled, phase 1–2 clinical trial (ABDALA Study). *EClinicalMedicine*. **46**, 101383. https://doi.org/10.1016/j.eclinm.2022.101383 (2022). Epub 2022 Apr 9. PMID: 35434578; PMCID: PMC8994669.
61. Yang, S. et al. Safety and immunogenicity of a recombinant tandem-repeat dimeric RBD-based protein subunit vaccine (ZF2001) against COVID-19 in adults: two randomised, double-blind, placebo-controlled, phase 1 and 2 trials. *Lancet Infect. Dis.* **21** (8), 1107–1119. https://doi.org/10.1016/S1473-3099(21)00127-4 (2021). Epub 2021 Mar 24. PMID: 33773111; PMCID: PMC7990482.
62. Dai, L. et al. ZF2001 Global Trial Group. Efficacy and Safety of the RBD-Dimer-Based COVID-19 Vaccine ZF2001 in Adults. N Engl J Med. ;386(22):2097–2111. doi: 10.1056/NEJMoa2202261. Epub 2022 May 4. PMID: 35507481; PMCID: PMC9127771. (2022).
63. Valdes-Balbin, Y. et al. Verez Bencomo V. SARS-CoV-2 RBD-Tetanus Toxoid Conjugate Vaccine induces a strong neutralizing immunity in Preclinical studies. *ACS Chem. Biol.* **16** (7), 1223–1233. https://doi.org/10.1021/acschembio.1c00272 (2021). Epub 2021 Jul 4. PMID: 34219448.
64. Chen, W. H. et al. Genetic modification to design a stable yeast-expressed recombinant SARS-CoV-2 receptor binding domain as a COVID-19 vaccine candidate. *Biochim. Biophys. Acta Gen. Subj.* **1865** (6), 129893. https://doi.org/10.1016/j.bbagen.2021.129893 (2021). Epub 2021 Mar 14. PMID: 33731300; PMCID: PMC7955913.
65. Thuluva, S. et al. Evaluation of safety and immunogenicity of receptor-binding domain-based COVID-19 vaccine (Corbevax) to select the optimum formulation in open-label, multicentre, and randomised phase-1/2 and phase-2 clinical trials. *EBioMedicine*. **83**, 104217 (2022). Epub 2022 Aug 12. PMID: 35970020; PMCID: PMC9372721.
66. Mahboob, T. et al. Development of SARS-CoV-2 vaccine: challenges and prospects. *Diseases*. **11** (2), 64. https://doi.org/10.3390/diseases11020064 (2023). PMID: 37092446; PMCID: PMC10123684.
67. Zepeda-Cervantes, J., Ramírez-Jarquín, J. O. & Vaca, L. Interaction between Virus-Like particles (VLPs) and Pattern Recognition Receptors (PRRs) from dendritic cells (DCs): toward Better Engineering of VLPs. *Front. Immunol.* **11**, 1100. https://doi.org/10.3389/fimmu.2020.01100 (2020). PMID: 32582186; PMCID: PMC7297083.
68. Collins, A. M. IgG subclass co-expression brings harmony to the quartet model of murine IgG function. *Immunol. Cell. Biol.* **94** (10), 949–954. https://doi.org/10.1038/icb.2016.65 (2016). Epub 2016 Aug 9. PMID: 27502143.
69. Gomes, C., Roesti, A., El-Turabi, E. S. & Bachmann, A. Type of RNA packed in VLPs impacts IgG class switching-implications for an Influenza Vaccine Design. *Vaccines (Basel)*. **7** (2), 47. https://doi.org/10.3390/vaccines7020047 (2019). PMID: 31167472; PMCID: PMC6630894.
70. Kaplan, C. et al. Th1 and Th2 cytokines regulate proteoglycan-specific autoantibody isotypes and arthritis. *Arthritis Res.* **4** (1), 54–58. https://doi.org/10.1186/ar383 (2002). Epub 2001 Oct 2. PMID: 11879537; PMCID: PMC64852.
71. Firacative, C. et al. Identification of T helper (th)1- and Th2-associated antigens of Cryptococcus neoformans in a murine model of pulmonary infection. *Sci. Rep.* **8**, 2681. https://doi.org/10.1038/s41598-018-21039-z (2018).
72. Bai, B. et al. Virus-like particles of SARS-like coronavirus formed by membrane proteins from different origins demonstrate stimulating activity in human dendritic cells. *PLoS One*. **3** (7), e2685. https://doi.org/10.1371/journal.pone.0002685 (2008). PMID: 18628832; PMCID: PMC2441860.
73. Dai, S., Zhang, T., Zhang, Y., Wang, H. & Deng, F. Zika Virus Baculovirus-Expressed Virus-Like Particles Induce Neutralizing Antibodies in Mice. Virol Sin. ;33(3):213–226. doi: 10.1007/s12250-018-0030-5. Epub 2018 May 17. PMID: 29774519; PMCID: PMC6013542. (2018).

74. Bosio, C. M. et al. Ebola and Marburg virus-like particles activate human myeloid dendritic cells. Virology. ;326(2):280-7. doi: (2004). https://doi.org/10.1016/j.virol.2004.05.025. PMID: 15302213.
75. Walls, A. C. et al. Elicitation of potent neutralizing antibody responses by designed protein nanoparticle vaccines for SARS-CoV-2. bioRxiv [Preprint]. 2020 Aug 12:2020.08.11.247395. doi: 10.1101/2020.08.11.247395. Update in: Cell. 2020;: PMID: 32817941; PMCID: PMC7430571.
76. Davis, M. et al. A C57BL/6 Mouse model of SARS-CoV-2 infection recapitulates age- and sex-based differences in human COVID-19 disease and recovery. Res Sq [Preprint]. 2022 Nov 14:rs.3.rs-2194450. doi: (2022). https://doi.org/10.21203/rs.3.rs-2194450/v1. Update in: Vaccines (Basel). ;11(1):47. doi: 10.3390/vaccines11010047. PMID: 36415465; PMCID: PMC9681052.
77. Darif, D. et al. The pro-inflammatory cytokines in COVID-19 pathogenesis: what goes wrong? *Microb. Pathog.* **153**, 104799. https://doi.org/10.1016/j.micpath.2021.104799 (2021). Epub 2021 Feb 18. PMID: 33609650; PMCID: PMC7889464.
78. Rabaan, A. A. et al. Role of inflammatory cytokines in COVID-19 patients: a review on Molecular mechanisms, Immune functions, Immunopathology and Immunomodulatory drugs to Counter Cytokine Storm. *Vaccines (Basel).* **9** (5), 436. https://doi.org/10.3390/vaccines9050436 (2021). PMID: 33946736; PMCID: PMC8145892.
79. Zhang, Q. et al. Inflammation and antiviral Immune Response Associated with severe progression of COVID-19. *Front. Immunol.* **12**, 631226. https://doi.org/10.3389/fimmu.2021.631226 (2021). PMID: 33679778; PMCID: PMC7930228.
80. Faraj, S. S., Jalal, P. J. & IL1β IL-6, and TNF-α cytokines cooperate to modulate a complicated medical condition among COVID-19 patients: case-control study. *Ann. Med. Surg. (Lond).* **85** (6), 2291–2297. https://doi.org/10.1097/MS9.0000000000000679 (2023). PMID: 37363608; PMCID: PMC10289607.

Acknowledgements

We would like to express our gratitude to Leda dos Reis Castilho from the Cell Culture Engineering Laboratory at COPPE/UFRJ (Rio de Janeiro, Brazil) for the generous donation of recombinant Spike protein for this study. We also thank the Laboratory of Celular Biology at the Butantan Institute (São Paulo, Brazil) for their assistance with negative-stain electron microscopy.We would also like to thank Dr. Ana Luiza Gibertoni Cruz, an infectious disease physician with a Master's in Public Health from Harvard and a PhD from the University of Oxford, and Dr. Daniel Cooke, a computational biologist, University of Oxford, for their essential assistance in reviewing and refining the language of this manuscript, which was crucial for ensuring the article's clarity and accuracy.

Author contributions

L.V - has implemented all experiments, data analysis, and wrote the paper draft.N.C, V.B.M, J.D.Q.S, A.L, W.A.P-S, L.F.S, D.L, R.D-C - have contributed to the experiments and revising of the paper.A.B, N.O.S.C, O.C-M, J.E.K, M.H.H - have contributed to the writing and revising of the paper. G.C-M - has supervised all experiments and contributed to the writing and revising of the paper.

Funding

The authors acknowledge the support provided by The São Paulo Research Foundation – FAPESP: GC-M: 2019/14526-0, 2020/04667-3; LV and GC-M: 2020/09404-0 (Post-doc Scholarship); NC and GC-M: 2021/03508-1 (PhD Scholarship); AL and GC-M: 2021/03102-5 (PhD Scholarship); WAPS and GC-M 2021/08468-8 (PhD Scholarship).

Declarations

Competing interests

The authors declare no competing interests.

Additional information

Supplementary Information The online version contains supplementary material available at https://doi.org/10.1038/s41598-024-76163-w.

Correspondence and requests for materials should be addressed to G.C.-M.